

Characterization of polymetamorphism in the Austroalpine basement east of the Tauern Window using garnet isopleth thermobarometry

F. GAIDIES,¹ R. ABART,² C. DE CAPITANI,¹ R. SCHUSTER,³ J. A. D. CONNOLLY⁴ AND E. REUSSER⁴

¹Department of Geosciences, University of Basel, Bernoullistrasse 30, CH-4056 Basel, Switzerland (fred.gaidies@unibas.ch)

²Institute of Geological Sciences, Free University of Berlin, Malteserstrasse 74-100, D-12249 Berlin, Germany

³Geological Survey of Austria, Neulinggasse 38, A-1031 Vienna, Austria

⁴Earth Sciences Department, Swiss Federal Institute of Technology, CH-8092 Zurich, Switzerland

ABSTRACT Garnet in metapelites from the Wölz and Rappold Complexes of the Austroalpine basement east of the Tauern Window typically shows two distinct growth zones. A first garnet generation usually forms the cores of garnet porphyroblasts and is separated by a prominent microstructural and chemical discontinuity from a second garnet generation, which forms rims of variable width. Whereas the rims were formed during the Eo-Alpine metamorphic overprint, the garnet cores represent remnants of at least two pre-Eo-Alpine metamorphic events. The pressure and temperature estimates obtained from garnet isopleth thermobarometry applied to the first growth increments of the pre-Eo-Alpine garnet cores from the Wölz and Rappold Complexes cluster into two distinct domains: (i) in the Wölz Complex, incipient growth of the first-generation garnet occurred at 4 ± 0.5 kbar and 535 ± 20 °C, (ii) in the Rappold Complex, incipient growth of the oldest garnet cores took place at 5.3 ± 0.3 kbar and 525 ± 15 °C. The Eo-Alpine garnet generation started to grow at 6.5 ± 0.5 kbar and 540 ± 10 °C. According to radiometric dating, the low-pressure garnet from the Wölz complex was formed during a Permian metamorphic event. The first-generation garnet of the Rappold Complex is probably of Variscan age.

Key words: Austroalpine basement; garnet; metapelite; Rappold Complex; Wölz Complex.

INTRODUCTION

The determination of pressure–temperature–time (*P–T–t*) paths from metamorphic mineral parageneses is an important tool in unravelling the development of orogenic belts (Spear, 1993). Garnet isopleth thermobarometry has been applied to derive *P–T* estimates from monometamorphic (e.g. Menard & Spear, 1993; Vance & Mahar, 1998; Stowell *et al.*, 2001; Zeh, 2001; Zeh & Holness, 2003; Evans, 2004; Kim & Bell, 2005) and polymetamorphic (e.g. Zeh *et al.*, 2004) rocks.

A prerequisite for the application of garnet isopleth thermobarometry is that thermodynamic equilibrium is maintained between the rim of the garnet and the rock matrix during garnet growth. In this case, the composition of successive garnet growth zones is solely determined by the *P–T* conditions as well as fluid composition for any given thermodynamically relevant bulk composition. The latter is defined as the volume domain in a rock, over which equilibrium is maintained during garnet growth. Garnet growth in previously unmetamorphosed hydrous rocks or in rocks that have only experienced low-grade metamorphism generally occurs by dehydration reactions. During dehydration, an aqueous fluid is likely to be present in

excess and, hence, reaction kinetics and material transport are expected to be fast. In such cases, chemical equilibrium is established rapidly and equilibrium domains may develop in the hand specimen or even on a larger scale (Carlson, 1989, 2001; Dohmen & Chakraborty, 2003). However, rocks that consist of prominent compositional banding may indicate the juxtaposition of different equilibrium domains, which has to be considered if the composition of the thermodynamically relevant bulk composition is to be determined.

Thermodynamic equilibrium between garnet and the rock matrix may be assumed, if garnet isopleth thermobarometry is applied to the incipient stages of garnet growth, i.e. if only the composition of garnet cores of the oldest garnet generation present in a rock is used. In this case, equilibrium-phase relations that are calculated by free-energy minimization for a system with specified bulk composition (e.g. de Capitani & Brown, 1987; Powell & Holland, 1993; Connolly & Petrin, 2002) and an internally consistent thermodynamic database (e.g. Berman, 1988; Gottschalk, 1997; Holland & Powell, 1998) can be used as theoretical predictions of the equilibrium assemblages that would develop if the corresponding rock maintained

equilibrium and the bulk composition is appropriate. The P – T conditions that prevailed during the initial stages of garnet growth can then be derived from comparison of the observed garnet compositions and the equilibrium assemblage diagrams, including contours for garnet composition, calculated for the appropriate bulk-rock composition.

A second prerequisite for the application of garnet isopleth thermobarometry is that the original growth zoning of garnet is preserved in its original state, i.e. that modification of the original chemical zoning pattern by intracrystalline diffusion is negligible. This is a reasonable assumption as long as amphibolite facies conditions are not surpassed, because of the exceedingly slow rates of cation diffusion in garnet (Chakraborty & Ganguly, 1992). Hence, for a persuasive modification of the original chemical pattern at low to moderate temperatures to occur, garnet has to be exposed to these temperatures for extraordinary long durations. In contrast, only the short-term exposure of garnet to temperatures exceeding amphibolite facies conditions prevents them from effective modification of the original zoning pattern. There is general agreement on the presumption that the chemical zoning patterns of garnet porphyroblasts provide reliable records of the P – T evolution up to upper amphibolite facies conditions (e.g. Ayres & Vance, 1997). However, Stowell *et al.* (1996) demonstrated that in addition to intracrystalline diffusion other processes such as Ca-metasomatism might affect the original growth zoning of garnet.

As a result of the considerably slow intracrystalline diffusion in garnet at low to moderate temperatures, the components which are incorporated into garnet during growth, are effectively removed from the rock matrix (e.g. Vance & Mahar, 1998; Evans, 2004). In general, certain components such as Mn or Fe are preferentially fractionated into garnet. This leads to a successive depletion of these components in the rock matrix and may change the effective bulk-rock composition during garnet growth. This effect is particularly pronounced if the modal amount of newly formed garnet is high. The fractionation effect must be accounted for, if garnet isopleth thermobarometry is used to reconstruct P – T paths from the compositions of successive garnet growth increments. The progressive modification of the thermodynamically relevant bulk-rock composition during garnet growth may be estimated from a Rayleigh fractionation model (Hollister, 1966; Atherton, 1968; Evans, 2004).

In this study, we present an application of garnet isopleth thermobarometry to polymetamorphic garnet porphyroblasts of metapelites from the Wölz and Rappold Complexes of the Austroalpine crystalline basement east of the Tauern Window (Niedere Tauern, Eastern Alps) (Table 1). It will be demonstrated that the application of garnet isopleth thermobarometry allows P – T estimates to be determined for incipient garnet growth of the oldest metamorphic garnet gen-

Table 1. Sample locations and GPS coordinates.

Sample	Coordinates ^a		Altitude (m)	Unit
	E	N		
10F03	014°13'15"	47°19'16"	2030	Wölz
11F03	014°13'20"	47°19'20"	2060	Wölz
12F03	014°13'20"	47°19'20"	2060	Wölz
16F03	014°13'00"	47°19'08"	1950	Wölz
28F03	014°15'44"	47°18'39"	2010	Wölz
29F03A + B	014°15'48"	47°18'49"	2020	Wölz
32F03	014°15'52"	47°19'03"	2230	Wölz
37F03	014°24'28"	47°23'17"	2060	Wölz
39F03	014°24'11"	47°23'24"	2040	Wölz
40F03-1	014°24'11"	47°23'25"	2060	Wölz
40F03-2	014°24'11"	47°23'25"	2060	Wölz
41F03	014°24'03"	47°23'29"	2090	Wölz
42F03	014°24'02"	47°23'29"	2100	Wölz
43F03	014°24'02"	47°23'29"	2100	Wölz
44F03	014°23'54"	47°23'33"	2130	Wölz
19F03	014°12'46"	47°18'53"	1790	Rappold
24F03	014°12'46"	47°18'42"	1825	Rappold
31F03	014°15'49"	47°19'00"	2170	Rappold
33F03	014°15'52"	47°19'06"	2265	Rappold
35F03	014°15'46"	47°19'15"	2170	Rappold

^aWorld Geodetic System 84 (WGS84).

erations preserved, employing bulk-rock chemistries and garnet as the only relic of the preexisting mineral parageneses. Furthermore, it will be shown that the integration of garnet isopleth thermobarometry with the Rayleigh fractionation model of Evans (2004) enables detailed P – T paths to be predicted for garnet growth in the course of different orogenic cycles. The results obtained help to discriminate between distinctive metamorphic events and, hence, provide insights into the polymetamorphic evolution in the Eastern Alps.

GEOLOGICAL SETTING

The Eastern Alps form a 500-km-long east–west-trending fold and thrust belt. They developed in the course of two distinct continent–continent collision events during the Cretaceous and Tertiary (Froitzheim *et al.*, 1996). According to Schmid *et al.* (2004), three major plate-tectonic units can be distinguished in the Eastern Alps: the Helvetic realm and the sub-Penninic nappes are considered to represent one major unit which corresponds to the former southern European margin. The Penninic nappes represent the Jurassic and Cretaceous oceanic crust and micro-continents, and the Austroalpine nappes represent the frontal part of the Apulian continental microplate. In the Cretaceous, the Apulian microplate experienced internal deformation because of a WNW–ESE-directed intracontinental collision event, which is referred to as the Eo-Alpine event. Cretaceous tectonics led to the formation of large décollement nappes in the uppermost crustal levels and substantial shortening and subduction in the deeper basement units. The northern and tectonically deeper units of the Austroalpine basement belong to the lower plate of the Cretaceous intracontinental subduction event and experienced metamor-

phism ranging from greenschist to eclogite facies conditions at *c.* 90 Ma (Thöni, 2002).

Conversely, the tectonically higher units in the southern part of the Austroalpine basement units pertain to the upper plate of the Cretaceous intracontinental subduction event. In general, they experienced metamorphic imprints during the Eo-Alpine collision event ranging from greenschist facies conditions at the base to anchizonal to diagenetic conditions in the uppermost parts (Schuster *et al.*, 2004). The Penninic nappes and the Austroalpine nappe pile overrode the former southern European margin in the course of the closure of the Penninic Ocean during the Tertiary.

The Austroalpine basement units in the Niedere Tauern (Fig. 1), which were part of the tectonic lower plate during Cretaceous orogeny, are primarily composed of paragneisses and metapelites with subordinate intercalations of amphibolites, quartzites, calcisilicate rocks and marbles. Because of widespread greenschist to amphibolite facies metamorphic overprint during the Eo-Alpine metamorphic event, low- to medium-grade parageneses of pre-Cretaceous age have largely been obliterated (e.g. Schuster & Thöni, 1996; Schuster & Frank, 1999; Schuster *et al.*, 2001, 2004).

The investigation of metamorphic assemblages from those parts of the Austroalpine realm which were less intensely affected during the Cretaceous yielded conditions ranging between 570 and 710 °C at <4 kbar during the Permo-Triassic (e.g. Habler & Thöni, 2001; Schuster *et al.*, 2001).

The Wölz and the tectonically overlying Rappold Complex are prominent lithostratigraphic units in the Niedere Tauern (Figs 1 & 2). Both complexes are separated from one another by a Cretaceous thrust fault and belong to the Upper Austroalpine basement nappes (Schmid *et al.*, 2004; Schuster *et al.*, 2004). Garnet porphyroblasts with two distinct growth zones in metapelites of the Wölz and Rappold Complexes demonstrate the polymetamorphic history of both units (e.g. Schuster & Thöni, 1996; Bernhard & Hoinkes, 1999; Schuster & Frank, 1999; Schuster *et al.*, 2001; Faryad & Hoinkes, 2003). Based on the microstructural relationship to the main schistosity and on radiometric age determinations it is inferred that the second garnet generation, which commonly constitutes rims enclosing the first-generation garnet, grew synchronously to the formation of the Eo-Alpine foliation (Abart & Martinelli, 1991; Schuster & Frank,

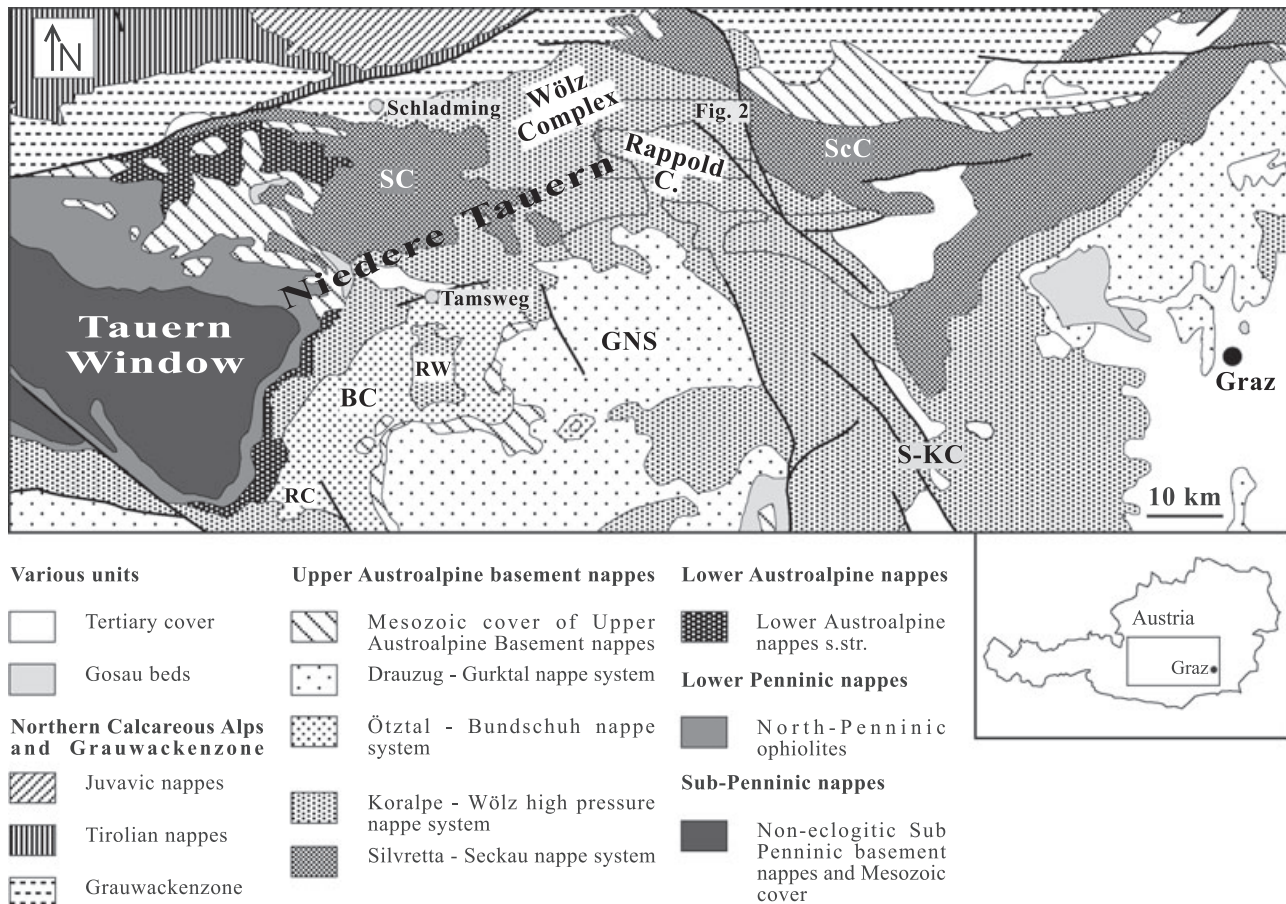


Fig. 1. Simplified tectonic map of the Austroalpine units to the east of the Tauern Window showing the location of the Wölz and Rappold Complexes. BC, Bundschuh Complex; GNS, Gurktal nappe system; SC, Schladming Complex; ScC, Seckau Complex; S-KC, Saualpe-Koralpe Complex. RW, Ramingstein Window and RC, Radenthein Complex are part of the Wölz Complex.

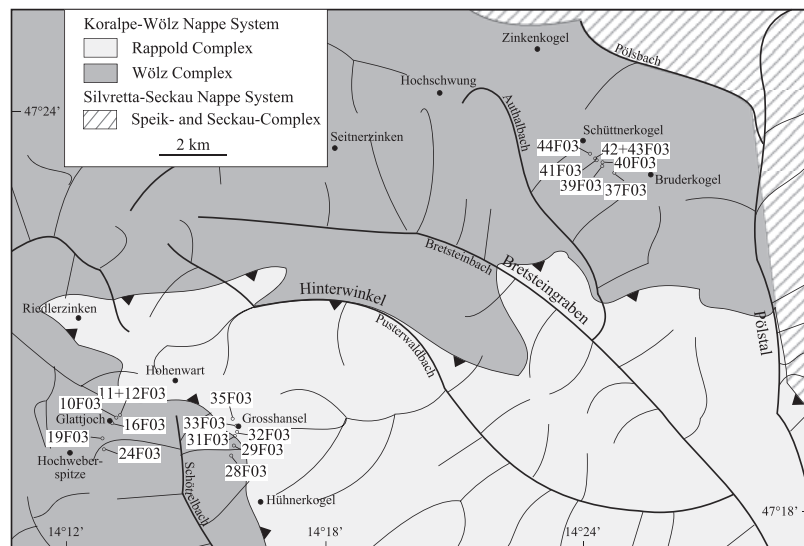


Fig. 2. Tectonic map of the study area showing sample locations.

1999) at $\sim 550\text{--}600\text{ }^{\circ}\text{C}$ and 10–12 kbar (e.g. Hoinkes *et al.*, 1999; Schuster & Frank, 1999; Faryad & Hoinkes, 2003).

In contrast, data on the formation conditions and ages are scarce for the first-generation garnet that forms the core of the garnet porphyroblasts. A garnet core from the Wölz Complex, which was dated to $269 \pm 4\text{ Ma}$ using the Sm–Nd garnet–whole-rock method (Schuster & Thöni, 1996; Schuster & Frank, 1999; Thöni, 2002), suggests the formation of the first-generation garnet during Permian times. As the first-generation garnet is the only remnant of Permian metamorphic assemblages in the Wölz Complex and in many cases, quartz and ilmenite are the only mineral inclusions in that garnet, detailed information about the P – T conditions during Permian metamorphism in the Wölz Complex are not known (e.g. Schuster & Frank, 1999; Faryad & Hoinkes, 2003).

From thermobarometry applied to inclusions of biotite, muscovite, plagioclase, quartz, ilmenite and rutile in first-generation garnet of a metapelite from the Rappold Complex, Faryad & Hoinkes (2003) derived P – T conditions of $\sim 540 \pm 15\text{ }^{\circ}\text{C}$ and $6.6 \pm 0.8\text{ kbar}$. The age of this pre-Eo-Alpine metamorphic event in the Rappold Complex is yet unknown. However, Sm–Nd garnet–whole-rock age determinations of garnet in metapegmatites of the Rappold Complex yielded $262 \pm 2\text{ Ma}$ and $288 \pm 4\text{ Ma}$ (Schuster & Thöni, 1996; Schuster *et al.*, 2001), indicating an enhanced geothermal gradient during the Permian in the Rappold Complex.

METHODS

Sample preparation and EPMA

To get an insight into the three-dimensional geometrical relationships among garnet porphyroblasts, serial

sections with a spacing of $\sim 0.6\text{--}0.8\text{ mm}$ were made from a representative sample domain of approximately $1 \times 2 \times 3\text{ cm}$ size of each rock sample. Cross-sections that contain garnet cores were located by selecting the three thin sections with the largest diameters of a single garnet porphyroblast. From these three thin sections, the one which yielded the highest content of X_{sps} [= $\text{Mn}/(\text{Fe}^{2+} + \text{Ca} + \text{Mg} + \text{Mn})$] in the central portion of the garnet cross-section, was considered to reflect the entire growth history including the incipient stages of garnet growth.

Electron probe micro-analysis was performed using a JEOL JXA-8600 at the Mineralogical and Petrographical Institute at the University of Basel and with JEOL JXA-8200 at ETH Zurich. The accelerating voltage was 15 kV for a beam current of 10 and 20 nA, respectively. Matrix corrections were performed with a PhiRhoZ routine. The garnet compositions were measured along two profiles that are perpendicular to each other for each of the three selected sections. Furthermore, concentration contour maps were obtained for Ca, Fe, Mg and Mn from calibrated X-ray maps and are shown in Figs 4, 6 and 8. The X_{grs} [= $\text{Ca}/(\text{Fe}^{2+} + \text{Ca} + \text{Mg} + \text{Mn})$] and X_{prp} [= $\text{Mg}/(\text{Fe}^{2+} + \text{Ca} + \text{Mg} + \text{Mn})$] contents are generally rather constant in the garnet core regions so that the spacing of isopleths is rather wide in these parts of the garnet. Compositional data for the incipient growth increments of three different garnet types are given in Table 2. The complete electron probe microanalysis (EPMA) data set is provided in Appendix A1.

Combustion analyses and WDXRF

Samples of $\sim 1\text{ kg}$, which were devoid of alteration and macroscopically detectable compositional heterogeneity, were carefully chosen. From these rock volumes, blocks of approximately $1 \times 2 \times 3\text{ cm}$ in size were

Table 2. Garnet core chemistry of samples from the Wölz and Rappold Complex.

Sample	Wölz Complex		Rappold Complex
	12F03	29F03B	35F03
SiO ₂	37.47	37.59	37.09
TiO ₂	0.05	0.16	0.06
Al ₂ O ₃	21.45	20.32	20.10
FeO	33.83	30.43	33.60
MnO	5.85	3.30	3.67
MgO	1.57	0.97	1.28
CaO	1.59	7.98	4.70
Total	101.81	100.75	100.50
Oxygen	12	12	12
Si	3.00	3.01	3.00
Ti	0.00	0.01	0.00
Al	2.02	1.92	1.92
Fe ³⁺	0.00	0.04	0.08
Fe ²⁺	2.26	2.00	2.19
Mn	0.40	0.22	0.25
Mg	0.19	0.12	0.15
Ca	0.14	0.69	0.41
Fe/(Fe + Mg)	0.92	0.95	0.93
Mg/(Fe + Mg)	0.08	0.06	0.07
X _{alm}	0.76	0.66	0.73
X _{ppp}	0.06	0.04	0.05
X _{grs}	0.05	0.23	0.14
X _{sps}	0.13	0.07	0.08

Table 3. Representative bulk-rock geochemical data of samples from the Wölz and Rappold Complex (wt%).

Sample	Wölz Complex		Rappold Complex	Average pelite ^a
	12F03	29F03B	35F03	
SiO ₂	57.51	64.04	48.02	59.77
TiO ₂	1.19	0.83	0.97	
Al ₂ O ₃	20.98	18.02	26.21	16.57
Fe ₂ O ₃	9.48	7.70	10.52	6.53
MnO	0.11	0.10	0.06	0.07
MgO	2.28	2.10	2.61	2.62
CaO	0.46	0.52	0.36	2.17
Na ₂ O	1.23	1.06	0.64	1.73
K ₂ O	3.73	3.43	5.84	3.53
H ₂ O	2.75	2.68	3.21	2.49
CO ₂	0.44	0.34	0.60	5.16
Total	100.16	100.82	99.04	100.64

^aFrom Symmes & Ferry (1991).

extracted for EPMA, and the rest was crushed and ground to a fine powder for combustion analysis using a LECO combustion analyser and to prepare glass pellets for bulk chemical analysis. The major element compositions were obtained by wavelength-dispersive X-ray fluorescence analysis (WDXRFA) using Bruker AXS SRS-3400. Both combustion analysis and WDXRFA were performed at the Mineralogical and Petrographical Institute at University of Basel. Representative whole-rock chemistries of three samples are shown in Table 3. The complete data set is provided in Appendix A2.

Garnet isopleth thermobarometry

Rock-specific equilibrium assemblage diagrams were calculated in the simplified model system MnO-Na₂O-CaO-K₂O-FeO-MgO-Al₂O₃-SiO₂-H₂O-TiO₂ (MnNC-

FMASHT). This choice of components ensures that most of the common rock-forming minerals in metapelites can be considered. TiO₂ was chosen as a system component to consider ilmenite. Ilmenite is ubiquitous in metapelites from the Wölz and Rappold Complexes. It may contain significant quantities of manganese and may thus have a strong influence on the low-temperature stability limit of garnet (e.g. Symmes & Ferry, 1992; Mahar *et al.*, 1997). Thermodynamic calculations were performed using the PERPLEX software (Connolly, 1990; Connolly & Petriani, 2002), adopting a gridded Gibbs free-energy minimization approach (Connolly, 2005), and the internally consistent and updated thermodynamic data set of Holland & Powell (1998) (thermodynamic database of THERMOCALC, version 3.21). The results obtained for three representative samples are presented in that study. Supplementary material, which covers the entire set of *P-T* phase diagram sections obtained for all the samples studied, is provided in Appendix A3.

The following notations, compositions (*w*, *x*, *y* and *z* are fractions varying between zero and unity and are determined as a function of pressure and temperature by free-energy minimization), and solution models have been employed: Grt [garnet, Fe_{3x}Ca_{3y}Mg_{3z}Mn_{3(1-x-y-z)}Al₂Si₃O₁₂; Holland & Powell, 1998], Chl [chlorite, (Mg_xFe_wMn_{1-x-w})_{5-y+z}Al_{2(1+y-z)}Si_{3-y+z}O₁₀(OH)₈; Holland *et al.*, 1998], AbPl [albite-rich side of the plagioclase solvus, Na_xCa_{1-x}Al_{2-x}Si_{2+x}O₈, *x* > 1/3; Newton *et al.*, 1980], AnPl [anorthite-rich side of the plagioclase solvus, Na_xCa_{1-x}Al_{2-x}Si_{2+x}O₈, *x* < 1/3; Newton *et al.*, 1980], Bt [biotite, K(Mg_xFe_yMn_{1-x-y})_{3-w}Al_{1+2w}Si_{3-w}O₁₀(OH)₂; Powell & Holland, 1999, extended to cover Fe and Mn solutions], St [staurolite, Mg_{4x}Fe_{4y}Mn_{4(1-x-y)}Al₁₈Si_{7.5}O₄₈H₄; Holland & Powell, 1998, extended to cover Mn-solutions], Clid [chloritoid, Mg_xFe_yMn_{1-x-y}Al₂SiO₅(OH)₂; White *et al.*, 2000, extended to cover Mn-solutions], Pheng [muscovite, K_xNa_{1-x}Mg_yFe_zAl_{3-2(y+z)}Si_{3+y+z}O₁₀(OH)₂, as described at <http://www.esc.cam.ac.uk/astaff/holland/ds5/muscovites/mu.html>], Camp [clinoamphibole, Ca₂Na_z(Mg_xFe_{1-x})_{3+2y+z}Al_{3-3y}Si_{7+y}O₂₂(OH)₂; Wei & Powell, 2003; White *et al.*, 2003], Ilm [ilmenite, Mg_xMn_yFe_{1-x-y}TiO₃, ideal ilmenite-geikielite-pyrophanite solution], Ky [kyanite, Al₂SiO₅], And [andalusite, Al₂SiO₅], Sil [sillimanite, Al₂SiO₅], Zo [zoisite, Ca₂Al₃Si₃O₁₂(OH)], Rt [rutile, TiO₂], Sa [sanidine, KAlSi₃O₈], Ttn [titanite, CaTiSiO₅], Qtz [quartz, SiO₂], and Mrg [margarite, CaAl₂Si₂O₁₀(OH)₂]. To save computational resources, the afchl endmember of chlorite was excluded because its contribution to the total energy of the solution is negligible. The influence of titanium on the stability of biotite (Kleemann & Reinhardt, 1994) was considered using the Ti-biotite solution model of Powell & Holland (1999) to the samples 12F03, 29F03B and 35F03. Both the results obtained by the application of the Ti-bearing and Ti-free biotite solution model (Powell & Holland, 1999) were compared. H₂O and

SiO₂ were considered as excess phases implying the presence of quartz and an aqueous fluid throughout the entire *P–T* range of interest. To consider the influence of changing H₂O and CO₂ activities during garnet growth, a graphite-buffered and carbon-, oxygen-, and hydrogen-bearing (GCOH-) fluid (Connolly & Cesare, 1993) was applied and compared with a *P–T* phase diagram section obtained with pure H₂O.

Although it is known that Zn strongly partitions into staurolite (e.g. Griffen, 1981; Proyer & Dachs, 2000), this feature could not be considered in our calculations because of the lack of thermodynamic data on Zn-staurolite. In the garnet analysed by EPMA, the recalculated Fe³⁺/Fe^{tot} varies between 0.00 and 0.04 (see Table 2), indicating that iron is predominantly present in the ferrous state. Thus, Fe³⁺ was not considered in our calculations.

The algorithm used in PERPLEX involves discretization of solid-solution compositions by series of so-called pseudocompounds with a fixed composition. For garnet solid solution, the spacing of the pseudocompounds was set to 0.2–0.3 mol.% for the respective garnet endmembers. For practical purposes, a pseudocompound spacing of 1–2.5 mol.% was chosen for chlorite and biotite solid solution. The database file, one solution-model file, and one input file used with PERPLEX is provided in Appendix A4.

The X_{sps} , X_{grs} and X_{alm} [=Fe²⁺/(Fe²⁺ + Ca + Mg + Mn)] isopleths were used as the three independent thermodynamic variables to describe the compositional variation of garnet in *P–T* space. The intersections of the isopleths that represent the observed garnet compositions are used to estimate the *P–T* conditions of the respective increment of garnet growth.

Calculation of the thermodynamically relevant bulk composition

To adequately predict the order of magnitude of the effect of chemical fractionation during garnet growth on garnet stability and composition, the method described by Evans (2004) is applied. According to Hollister (1966), the following relation is used to account for chemical fractionation:

$$C_{\text{MnO}}^{\text{Grt}} = C_{\text{MnO}}^{\text{rock}} \cdot k_d(1 - M)^{k_d - 1},$$

where $C_{\text{MnO}}^{\text{Grt}}$ is the weight fraction of MnO in garnet, $C_{\text{MnO}}^{\text{rock}}$ is the initial weight fraction of MnO in the rock, k_d is the distribution coefficient by weight of MnO between garnet and the rock matrix, and M corresponds to the weight fraction of garnet that has already crystallized in the rock. The amount of garnet crystallized from the above relation was calculated for several compositions along the microprobe traverses presented in this study. The garnet–matrix distribution coefficient for Mn k_d was assumed constant during garnet growth and was approximated by the ratio between $C_{\text{MnO}}^{\text{Grt}}$ in the oldest garnet portion and $C_{\text{MnO}}^{\text{rock}}$ of

the unfractionated bulk-rock chemistry. This is justified by the notion that neither temperature nor equilibrium-phase relations change drastically during the stage of incipient garnet growth. The bulk fractionation is obtained from integration over the successive growth increments (Fig. 11). The chemical shift of the thermodynamically relevant bulk composition of the rock matrix is finally obtained by subtraction of the material that is fractionated into garnet from the respective bulk-rock composition. The M values calculated for different points within the garnet porphyroblasts, as well as the corresponding garnet and matrix compositions are given in Tables 4, 5 and 6.

SAMPLE DESCRIPTION

Twenty-one samples are discussed in this study and were taken from both the Wölz and the Rappold

Table 4. Garnet composition at points (1) to (4) of a garnet from the Wölz Complex with two growth zones (sample 12F03) and composition of the bulk chemistries corrected for chemical fractionation during garnet growth.

	Normalized composition of garnet point (in wt%)			
	(1)	(2)	(3)	(4)
SiO ₂	36.80	36.73	36.85	36.99
TiO ₂	0.05	0.05	0.02	0.07
Al ₂ O ₃	21.07	21.13	21.14	21.31
FeO	33.23	33.77	35.03	30.71
MnO	5.75	5.16	3.75	2.98
MgO	1.55	1.66	1.73	1.25
CaO	1.56	1.51	1.48	6.70
Total	100.00	100.00	100.00	100.00
Oxygen	12	12	12	12
Si	3.00	2.99	3.00	2.98
Ti	0.00	0.00	0.00	0.00
Al	2.02	2.03	2.03	2.02
Fe ³⁺	0.00	0.00	0.00	0.02
Fe ²⁺	2.26	2.30	2.38	2.05
Mn	0.40	0.36	0.26	0.20
Mg	0.19	0.20	0.21	0.15
Ca	0.14	0.13	0.13	0.58
Fe/(Fe + Mg)	0.92	0.92	0.92	0.93
Mg/(Fe + Mg)	0.08	0.08	0.08	0.07
X_{alm}	0.76	0.77	0.80	0.69
X_{prp}	0.06	0.07	0.07	0.05
X_{grs}	0.05	0.04	0.04	0.19
X_{sps}	0.13	0.12	0.09	0.07
M^{a}	0.001	0.003	0.009	0.013

	Normalized effective bulk chemistry for the growth of garnet (in wt%)		
	(1) ^{b,c}	(2) ^c	(3) ^c
SiO ₂	59.89	59.93	60.07
TiO ₂	1.24	1.24	1.25
Al ₂ O ₃	21.85	21.85	21.85
FeO	8.89	8.84	8.69
MnO	0.11	0.10	0.08
MgO	2.37	2.38	2.38
CaO	0.48	0.48	0.47
Na ₂ O	1.28	1.28	1.29
K ₂ O	3.88	3.89	3.91
Total	100.00	100.00	100.00

^aWeight fraction of crystallized garnet.

^bCorresponds to unfractionated bulk-rock chemistry in Table 3.

^cFor $k_d = 55$.

Table 5. Garnet composition at points (1) to (3) of a garnet from the Rappold Complex with two growth zones (sample 35F03) and composition of the bulk chemistries corrected for chemical fractionation during garnet growth.

	Normalized composition of garnet point (in wt%)		
	(1)	(2)	(3)
SiO ₂	36.91	36.98	36.91
TiO ₂	0.05	0.18	0.06
Al ₂ O ₃	20.00	20.17	20.24
FeO	33.44	33.48	36.76
MnO	3.65	3.21	1.07
MgO	1.28	1.35	1.73
CaO	4.68	4.63	3.24
Total	100.00	100.00	100.00
Oxygen	12	12	12
Si	3.00	3.00	3.00
Ti	0.00	0.01	0.00
Al	1.92	1.93	1.94
Fe ³⁺	0.08	0.05	0.06
Fe ²⁺	2.19	2.23	2.44
Mn	0.25	0.22	0.07
Mg	0.15	0.16	0.21
Ca	0.41	0.40	0.28
Fe/(Fe + Mg)	0.93	0.93	0.92
Mg/(Fe + Mg)	0.07	0.07	0.08
X _{alm}	0.73	0.74	0.81
X _{prp}	0.05	0.05	0.07
X _{grs}	0.14	0.13	0.09
X _{sps}	0.08	0.07	0.03
M ^a	0.000	0.002	0.020

	Normalized effective bulk chemistry for the growth of garnet (in wt%)		
	(1) ^b	(2) ^c	(3) ^c
SiO ₂	50.98	51.01	51.27
TiO ₂	1.03	1.03	1.05
Al ₂ O ₃	27.83	27.84	27.98
FeO	10.06	10.01	9.54
MnO	0.06	0.06	0.02
MgO	2.77	2.77	2.80
CaO	0.38	0.37	0.31
Na ₂ O	0.68	0.68	0.69
K ₂ O	6.20	6.21	6.33
Total	100.00	100.00	100.00

^aWeight fraction of crystallized garnet.^bCorresponds to unfractionated bulk-rock chemistry in Table 3.^cFor $k_d = 61$.

Complexes. Their geographical locations are given in Table 1 and Fig. 2. Three samples, which are considered as being representative of the entire set of samples, are described in some detail. Samples 12F03 (Fig. 3a) and 29F03B (Fig. 3b) are micaschists of the Wölz Complex with garnet grains containing two distinct growth zones and one growth zone, respectively. The sample 35F03 is a garnet-bearing metapelite of the Rappold Complex with polyphase garnet porphyroblasts (Fig. 3c).

Metapelite with polyphase garnet porphyroblasts from the Wölz Complex (sample 12F03)

The rock-matrix is composed of quartz, biotite, muscovite, tourmaline, ilmenite, rutile, retrograde chlorite and plagioclase. Biotite, muscovite and ilmenite define

Table 6. Garnet composition at points (1) to (3) of a garnet from the Wölz Complex with a single growth zone (sample 29F03) and composition of the bulk chemistries corrected for chemical fractionation during garnet growth.

	Normalized composition of garnet point (in wt%)		
	(1)	(2)	(3)
SiO ₂	37.31	37.33	37.45
TiO ₂	0.16	0.21	0.12
Al ₂ O ₃	20.17	20.25	20.34
FeO	30.20	30.54	32.25
MnO	3.28	2.38	0.90
MgO	0.96	1.05	1.50
CaO	7.92	8.23	7.44
Total	100.00	100.00	100.00
Oxygen	12	12	12
Si	3.01	3.01	3.01
Ti	0.01	0.01	0.01
Al	1.92	1.92	1.93
Fe ³⁺	0.04	0.03	0.04
Fe ²⁺	2.00	2.03	2.13
Mn	0.22	0.16	0.06
Mg	0.12	0.13	0.18
Ca	0.69	0.71	0.64
Fe/(Fe + Mg)	0.95	0.94	0.92
Mg/(Fe + Mg)	0.06	0.06	0.08
X _{alm}	0.66	0.67	0.71
X _{prp}	0.04	0.04	0.06
X _{grs}	0.23	0.24	0.21
X _{sps}	0.07	0.05	0.02
M ^a	0.001	0.011	

	Normalized effective bulk chemistry for the growth of garnet (in wt%)		
	(1) ^b	(2) ^c	(3) ^c
SiO ₂	66.00	66.33	67.16
TiO ₂	0.86	0.86	0.88
Al ₂ O ₃	18.57	18.55	18.50
FeO	7.15	6.87	6.16
MnO	0.10	0.07	0.03
MgO	2.16	2.18	2.20
CaO	0.54	0.45	0.25
Na ₂ O	1.09	1.11	1.14
K ₂ O	3.53	3.58	3.68
Total	100.00	100.00	100.00

^aWeight fraction of crystallized garnet.^bCorresponds to unfractionated bulk-rock chemistry in Table 3.^cFor $k_d = 34$.

the pervasive foliation of the rock. The garnet porphyroblasts, which are up to 6 mm in diameter, are composed of two distinct growth zones. Abundant inclusions of finely dispersed graphite and ilmenite are concentrated along the boundaries between the two growth zones, which makes it easy to discern them even macroscopically.

The first-generation garnet is ~4 mm in diameter and contains inclusions of quartz, ilmenite, tourmaline and small muscovite grains. The second-generation garnet is ~1.5 mm in size and forms rims enclosing the first-generation garnet. Mineral inclusions of ilmenite, rutile, tourmaline, muscovite and quartz are perceived in the second-generation garnet. Additionally, an intense graphitic pigmentation is observed in the inner portions, which decreases towards the outer portions of the rim. Similarly, the abundance of ilmenite

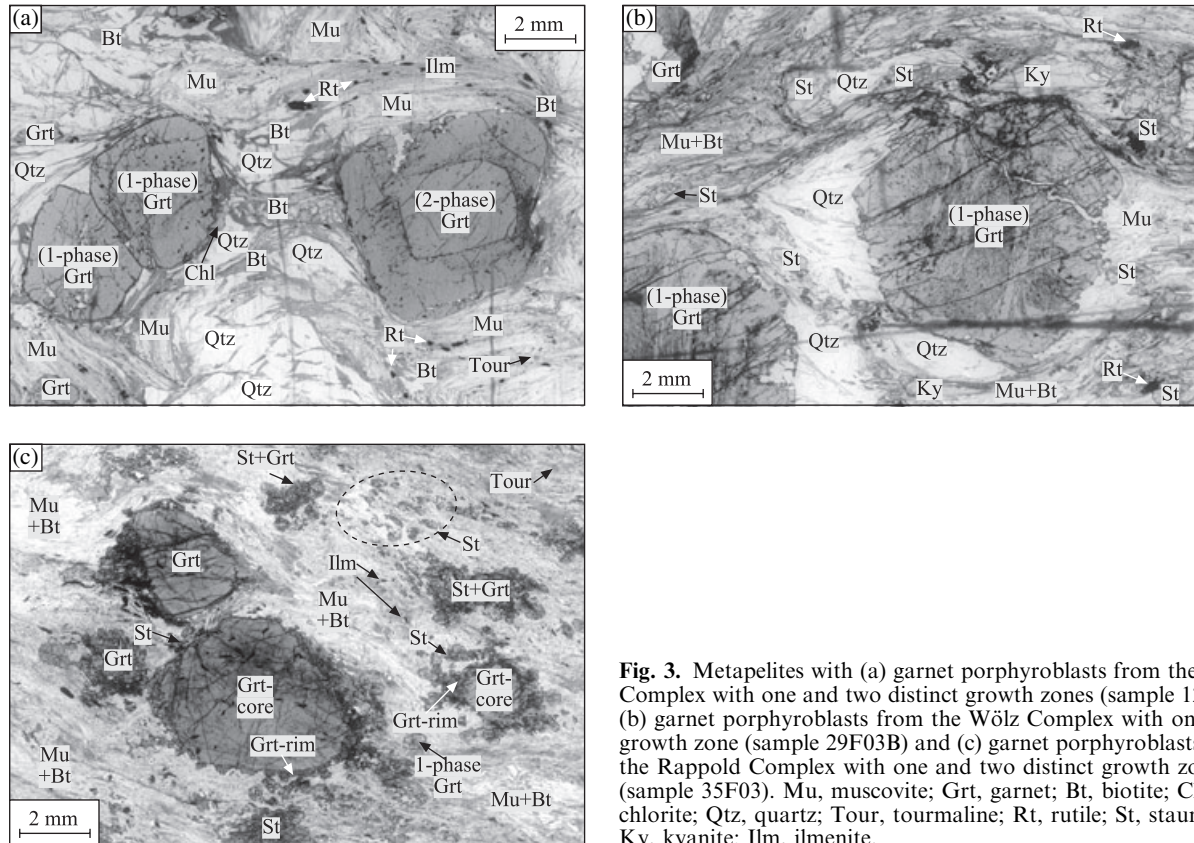


Fig. 3. Metapelites with (a) garnet porphyroblasts from the Wölz Complex with one and two distinct growth zones (sample 12F03), (b) garnet porphyroblasts from the Wölz Complex with one growth zone (sample 29F03B) and (c) garnet porphyroblasts from the Rappold Complex with one and two distinct growth zones (sample 35F03). Mu, muscovite; Grt, garnet; Bt, biotite; Chl, chlorite; Qtz, quartz; Tour, tourmaline; Rt, rutile; St, staurolite; Ky, kyanite; Ilm, ilmenite.

decreases outwards whereas the abundance of rutile increases (Fig. 5).

Metapelite with garnet porphyroblasts with only a single growth zone from the Wölz Complex (sample 29F03B)

The typical matrix mineral assemblage is quartz, muscovite, rutile, plagioclase and biotite. Kyanite porphyroblasts with undulatory extinction are commonly observed. They are up to 8 mm long and are often intergrown with staurolite porphyroblasts. They contain abundant inclusions of rutile and graphite. The garnet porphyroblasts are up to 8 mm in diameter and only show a single growth zone (Fig. 3b). Garnet inclusion suites are dominated by graphite, ilmenite, rutile, quartz, tourmaline, clinozoisite and allanite. The inclusions of ilmenite display, when elongate, a pre-existing foliation but are not found when rutile inclusions appear in the garnet rim. In few cases, inclusions of kyanite are observed in the outermost parts of garnet. Graphite inclusions are elongated and aligned, which together with ilmenite presumably represent a foliation that existed during garnet growth. Based on their microstructural relationship to the main schistosity, it is deduced that the garnet porphyroblasts grew at the same time as the Eo-Alpine foliation.

Metapelite with polyphase garnet porphyroblasts from the Rappold Complex (sample 35F03)

Biotite and muscovite, which trace the main foliation of the rock, as well as ilmenite, tourmaline, quartz and minor plagioclase, are the most abundant minerals of the matrix. Furthermore, up to 1-mm-size strongly resorbed staurolite blasts with abundant finely dispersed graphitic inclusions are observed, which occasionally rim the first growth zone of garnet porphyroblasts. Equilibrium textures are observed between staurolite and the first-generation garnet including straight interphase boundaries.

The two growth zones of garnet porphyroblasts differ significantly in size (Figs 8 & 9). The first generation is strongly graphitic and up to 7 mm in diameter (Fig. 3c). Ilmenite (up to 0.5 mm in size), quartz, muscovite, small chloritoid grains, tourmaline, as well as biotite in the outermost portions were observed as mineral inclusions in the first-generation garnet. The needle-shaped tourmaline grains and the graphite inclusions, when elongate, are generally parallel or sub-parallel to the included fabric.

The second-generation garnet is present as single-phase individual crystals and as a <1-mm-wide overgrowth on the large garnet cores enclosing quartz, tourmaline, ilmenite, biotite and muscovite (Fig. 9). In

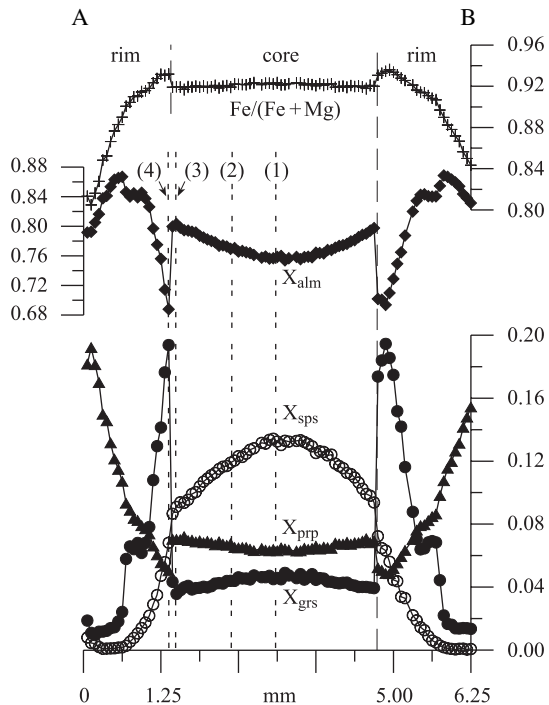


Fig. 4. Compositional profile across a garnet porphyroblast with two growth zones (sample 12F03, Wölz Complex). Note the sharp increase of grossular and concomitant decrease of almandine contents at the transition from the first to the second growth zone. P - T estimates for points (1) to (4) are given in Fig. 12.

several cases, indications of the replacement of staurolite by the second-generation garnet are observed.

RESULTS

Garnet chemistry

Polyphase garnet porphyroblasts from the Wölz Complex (sample 12F03)

The chemical composition of the first-generation garnet is characterized by a shallow continuous increase of X_{alm} and X_{prp} from the centre towards the rim, whereas $Fe/(Fe + Mg)$, X_{sps} and X_{grs} decrease (Fig. 4). The X_{sps} isopleths in Fig. 5 document the almost euhedral growth zoning pattern and only the 0.08 X_{sps} isopleth shows a local irregularity.

The transition between the first- and the second-generation garnet is characterized by a rapid increase of X_{grs} from ~ 0.04 at the outermost part of the core to more than 0.17 at the innermost portion of the rim (Fig. 4). Furthermore, X_{alm} and X_{prp} drop off sharply from ~ 0.80 to 0.70 and from 0.07 to ~ 0.05 , respectively. $Fe/(Fe + Mg)$ increases from ~ 0.92 to 0.93 at the transition between the inner and outer garnet growth zone.

The compositional gradients of the second-generation garnet are much larger than in the first-generation

garnet. X_{grs} shows a sharp outward decrease to values of ~ 0.01 to 0.02 at the outer edge. X_{prp} is somewhat lower in the innermost portion of the second-generation garnet (~ 0.05) compared with that in the outermost portion of the first-generation garnet (~ 0.07) and it shows a continuous outward increase to 0.16 to 0.20 at the outer edge of the rim. In places, the innermost portion of the second-generation garnet is characterized by a short stage with increasing $Fe/(Fe + Mg)$ and X_{grs} and a concomitant decrease in X_{alm} , X_{prp} and X_{sps} (see right-hand side of the profile in Fig. 4). In the central portion of the garnet rim, a 'shoulder' in the X_{grs} profile, which interrupts the general trend of outward falling X_{grs} , is observed. X_{alm} is relatively low in the innermost and outermost portions of the second-generation garnet and passes through a maximum in the central portion. A decrease in X_{prp} and a concomitant increase in $Fe/(Fe + Mg)$ is commonly observed in the outermost, several tens of micrometres wide zone of the rim (see left-hand side of the profile in Fig. 4).

Garnet porphyroblasts from the Wölz Complex with only a single growth zone (sample 29F03B)

In the core region of the garnet, the concentration of X_{grs} is substantially higher and X_{alm} and X_{prp} are lower than in the central portion of the first-generation garnet of polyphase garnet from the Wölz Complex (Figs 4 & 6). Furthermore, X_{grs} and $Fe/(Fe + Mg)$ decrease more steeply and X_{alm} as well as X_{prp} rise more rapidly from core to rim. Qualitatively, the zoning pattern of the one-phase garnet is similar to the zoning pattern of the second-generation garnet of polyphase garnet porphyroblasts of the Wölz Complex. The composition of the innermost portion of the one-phase garnet (Fig. 6) closely resembles the composition of the earliest portion of the second-generation garnet (Fig. 4). The number of mineral inclusions (Fig. 7) and the fluctuations in X_{grs} and X_{alm} (Fig. 6) are, however, higher in the one-phase garnet than in the second-generation garnet of the polyphase garnet.

Polyphase garnet porphyroblasts from the Rappold Complex (sample 35F03)

The X_{grs} , X_{sps} and $Fe/(Fe + Mg)$ of the first-generation garnet decrease, whereas X_{alm} and X_{prp} increase from the centre outwards (Fig. 8). In their outermost growth increments, the first-generation garnet shows a local maximum in X_{alm} . In this respect, it is similar to the second-generation garnet of the polyphase garnet from the Wölz Complex (Fig. 4). The first-generation garnet from the Rappold Complex is markedly more compositionally heterogeneous than the garnet core phase from the Wölz Complex. A condensation of the X_{sps} isopleths in the upper right portion (Fig. 9) is observed.

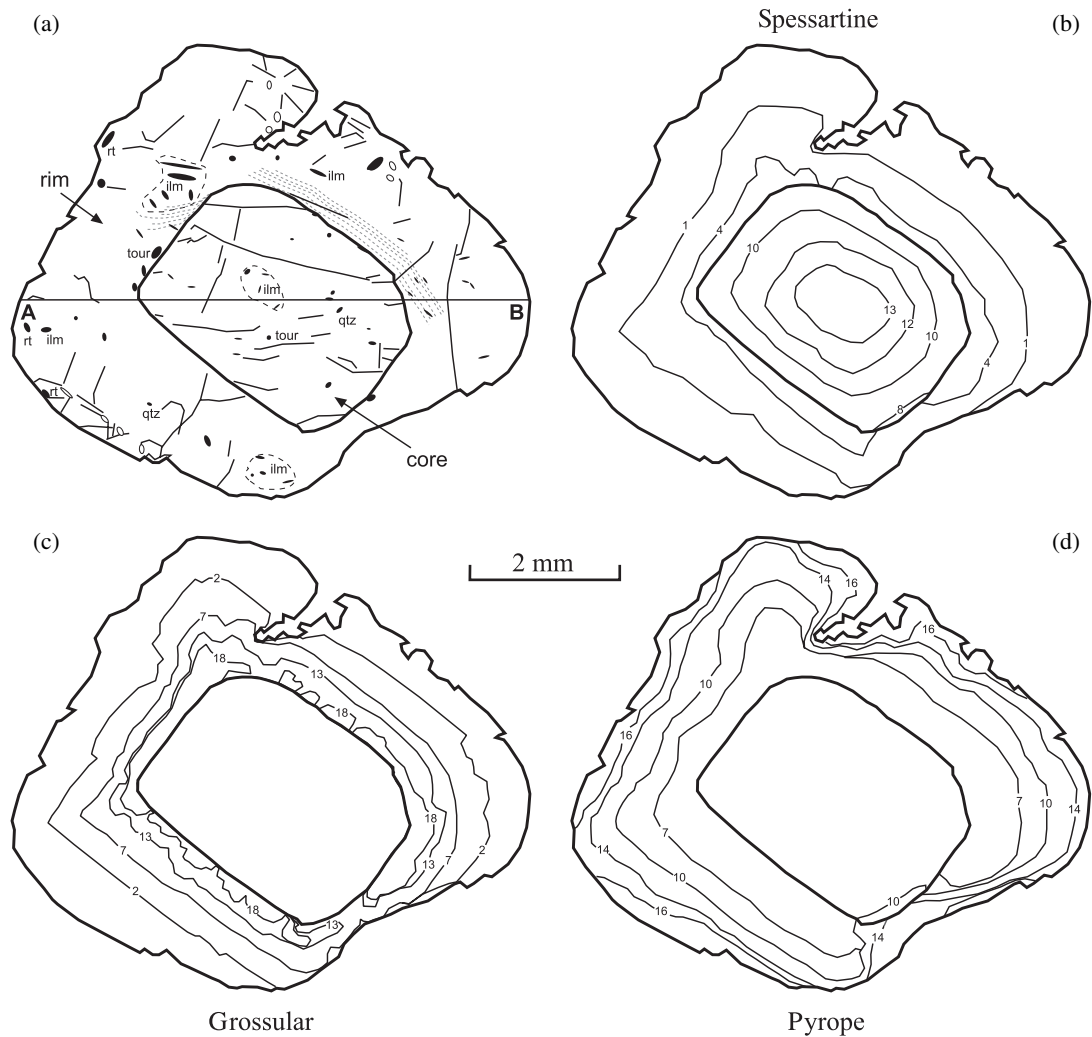


Fig. 5. (a) Textural and (b–d) compositional maps (in mol.%) of a garnet porphyroblast from the Wölz Complex with two growth zones (sample 12F03). Rutile appears at the outermost rim of the second-generation garnet, and ilmenite disappears at the same time. Small dashed lines represent graphitic pigmentation, which is restricted to the inner part of the second-generation garnet. The location of the profile A–B as shown in Fig. 4 is indicated.

In its innermost growth increment, the second-generation garnet shows higher values of X_{grs} than the first-generation garnet. The higher values of X_{grs} mark the transition between garnet core and rim. Within the garnet rim, X_{ilm} shows a substantial outward increase. In the outermost 10–20 μm , $\text{Fe}/(\text{Fe} + \text{Mg})$ increases sharply, with a concomitant decrease in X_{prp} .

Whole-rock chemistry

The bulk-rock compositions and the compositions of the garnet cores, which were used for garnet isopleth thermobarometry, are plotted in AFM and ACF diagrams in Fig. 10. The composition of the average pelite of Symmes & Ferry (1991) (Table 3), which is very similar to the composition of the average low-grade pelite of Shaw (1956), is shown for reference. Although

there is some scatter in the data, on average, the garnet-bearing metapelites of the Wölz and Rappold Complexes are similar in terms of their compositions. In the AFM diagram, all samples show distinctly lower relative concentrations of MgO than the average pelite of Symmes & Ferry (1991), and in the ACF diagram, they generally plot at somewhat higher A-values than the reference sample (Fig. 10). The compositions of garnet cores differ significantly from the average bulk-rock compositions. In the AFM projection, the compositions of garnet cores are at higher X_{Fe} than the respective bulk rock and they are at lower A-values in the ACF diagram. It is interesting to note that the compositions of garnet cores from the Wölz Complex define a linear trend in the ACF diagram, which represents variable C/F ratios at constant A value. This indicates that the values of X_{grs} are highly

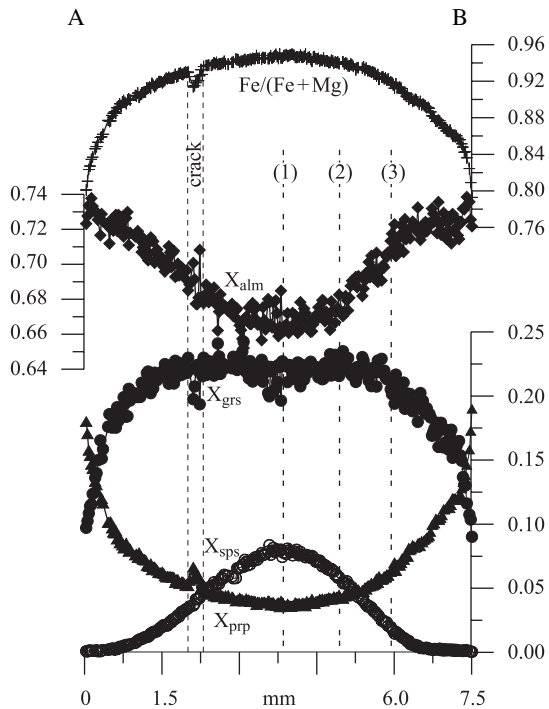


Fig. 6. Compositional profile across a garnet porphyroblast from the Wölz Complex with one growth zone (sample 29F03B). P – T estimates for points (1), (2) and (3) are given in Fig. 14.

variable in garnet cores from the Wölz Complex (Fig. 10b). In contrast, garnet cores from the Rappold Complex do not show any variation in their C/F ratios.

P – T estimates

The first-generation garnet of polyphase garnet from the Wölz Complex

Figure 12a–c illustrates the variation of garnet composition with pressure and temperature. Compositional isopleths were calculated for the original bulk-rock composition of sample 12F03 obtained from XRF analysis without correction for the effect of chemical fractionation associated with garnet growth (solid lines) and for the effective bulk composition that corresponds to the garnet growth stage represented by point (3) in Fig. 4 (dashed lines). The shift of the garnet stability field and of the compositional isopleths produced by chemical fractionation is minute for this specific sample. The effect of chemical fractionation at point (2) of Fig. 4 is not shown in Fig. 12a–c for the sake of legibility, but it is given in Table 4.

The isopleths corresponding to the garnet compositions of the growth stages represented by points (1), (2) and (3) of Fig. 4 are shown in Fig. 12d. For the incipient stages of garnet growth (point 1), the isopleths intersect close to the low-temperature stability limit of

garnet. The centre of the area of isopleth intersection is at ~ 4 kbar and 540 °C; this reflects the conditions during incipient garnet growth. As the influence of chemical fractionation during the growth stages (1) to (3) (Fig. 4) on garnet stability and composition is negligible for this particular rock sample, equilibrium-phase relations calculated for the bulk-rock composition of sample 12F03 (Table 3) are valid for the three garnet growth stages studied (Fig. 12e). The area of isopleth intersection that corresponds to incipient garnet growth in sample 12F03 [point (1) in Fig. 4] occurs in the stability field of the assemblage garnet, staurolite, chlorite, albite-rich plagioclase, quartz, ilmenite and muscovite. The P – T estimates obtained for incipient garnet growth of other first-generation garnet from the Wölz Complex yield conditions of $\sim 4 \pm 0.5$ kbar and 535 ± 20 °C (Fig. 15). The P – T conditions derived from the composition of the outermost portion of the first-generation garnet [point (3)] are 4.3 kbar and ~ 550 °C. The equilibrium assemblage remained unchanged during garnet growth from point (1) to point (3) (Figs 4 & 12e).

The second-generation garnet of polyphase garnet from the Wölz Complex (sample 12F03)

Point (4) of the compositional profile depicted in Fig. 4 pertains to the second-generation garnet in the Wölz Complex. The effects on the effective bulk composition of partial resorption of the garnet core and of successive fractionation during rim growth cannot be quantified. This is why the effective bulk composition that was calculated for point (3) (Table 4) was used for garnet isopleth thermobarometry. The resulting P – T estimates are at ~ 6.25 kbar and 530 °C for the growth stage represented by point (4) (Fig. 12e) and occur in the assemblage garnet, chlorite, muscovite, albite-rich plagioclase, quartz and ilmenite.

The one-phase garnet from the Wölz Complex (sample 29F03B)

Garnet isopleth thermobarometry yielded ~ 7.0 kbar and 530 °C as the conditions during incipient growth (Fig. 14). Calculated phase relations indicate that incipient garnet growth occurred in the assemblage garnet, chlorite, muscovite, albite-rich plagioclase, quartz and ilmenite. On average, conditions of $\sim 6.5 \pm 0.5$ kbar and 540 ± 10 °C are obtained from the central portions of other one-phase garnet from the Wölz Complex (Fig. 15).

Taking into account the effect of chemical fractionation during garnet growth, conditions of ~ 7.2 kbar and 535 °C and ~ 8.7 kbar and 550 °C have been derived for the growth stages represented by the points (2) and (3), respectively (see compositional profile illustrated in Fig. 6). The predicted equilibrium assemblage of point (3) is composed of muscovite, biotite, chlorite, ilmenite, garnet and quartz.

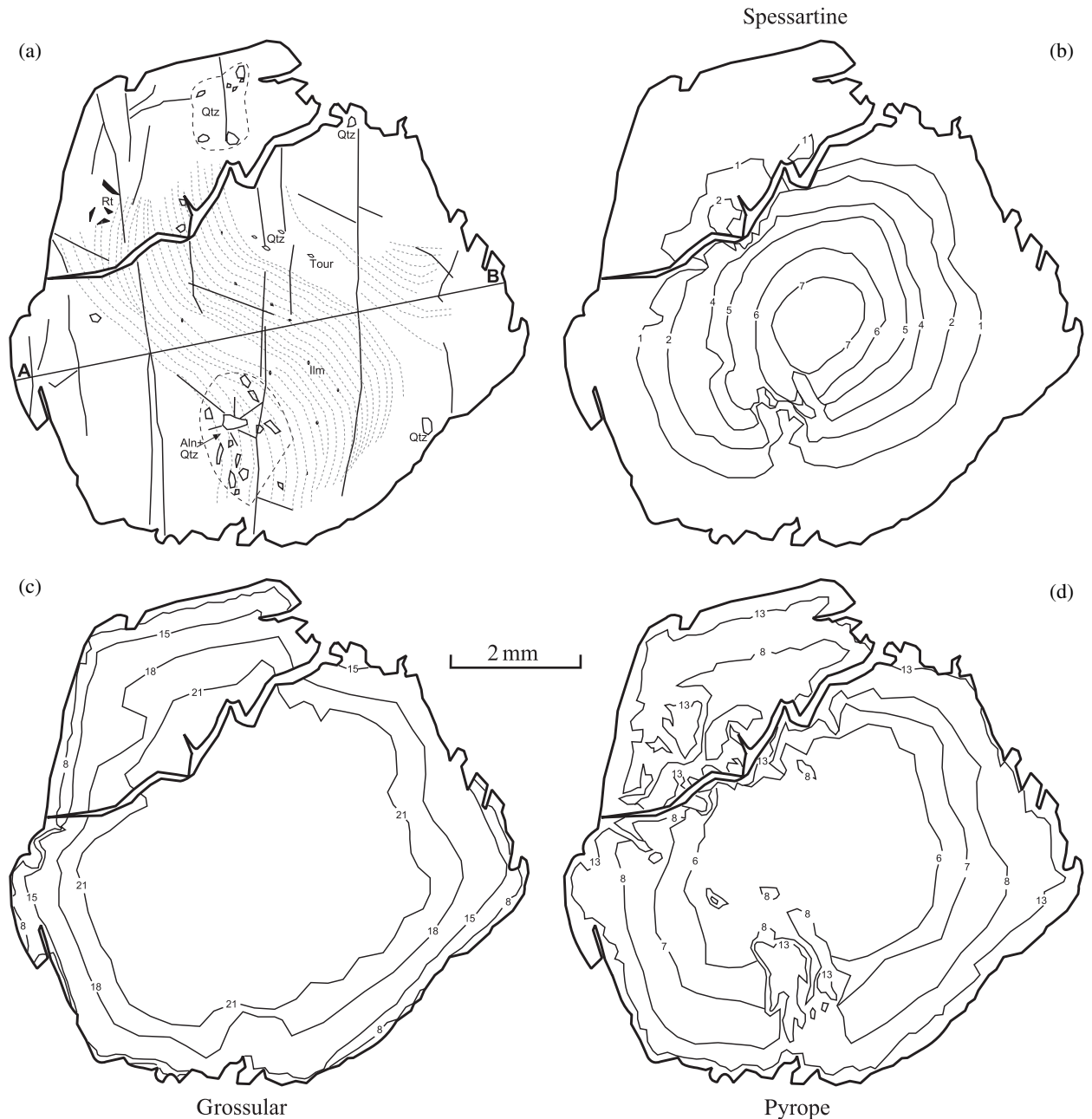


Fig. 7. (a) Textural and (b–d) compositional maps (in mol.%) of a garnet porphyroblast from the Wölz Complex with one growth zone (sample 29F03B). The location of the profile A–B as shown in Fig. 6 is indicated. The original growth zoning is modified along cracks and around mineral inclusions. Note the presence of allanite and the radial cracks surrounding it. The small dashed lines indicate an intense ‘s-shaped’ graphitic pigmentation, which disappears in the outermost portion of the garnet.

The first-generation garnet of polyphase garnet from the Rappold Complex (sample 35F03)

From the composition of the oldest growth increment conditions of ~ 5.2 kbar and 535 °C have been derived (Fig. 13). The corresponding equilibrium assemblage consists of garnet, chloritoid, chlorite, muscovite, albite-rich plagioclase, quartz and ilmenite. As shown in Fig. 15, the cores of other first-generation garnet from

the Rappold Complex yield P – T conditions of $\sim 5.3 \pm 0.3$ kbar and 525 ± 15 °C. The P – T conditions calculated for the growth stage represented by point (2) are ~ 5.4 kbar and 535 °C; this is within uncertainties identical to the conditions obtained for incipient garnet growth. For point (3), P – T conditions of ~ 5 kbar and 550 °C and the assemblage garnet, chlorite, muscovite, staurolite, albite-rich plagioclase, ilmenite and quartz are derived. The area of isopleth

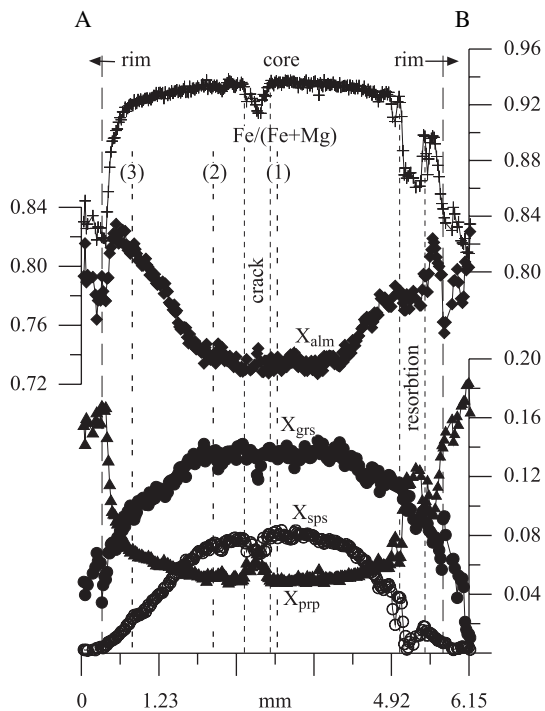


Fig. 8. Compositional profile across a garnet porphyroblast from the Rappold Complex with two growth zones (sample 35F03). The increase in the grossular content at the outer parts of the garnet marks the transition between the two growth zones. P - T estimates for points (1), (2) and (3) are given in Fig. 13.

intersection is comparatively large for this growth stage, and the uncertainties are accordingly large.

DISCUSSION

P - T estimates for incipient garnet growth

In medium grade metamorphic schists and gneisses, X_{grs} is sensitive to pressure during garnet growth (e.g. Kretz, 1964; Koziol & Newton, 1988, 1989). From the observation that the $\text{CaO}/(\text{CaO} + \text{FeO} + \text{MgO} + \text{MnO})$ ratios of first growth increments of the first- and the second-generation garnet from the Wölz Complex vary systematically despite relatively constant bulk-rock compositions (Fig. 10), it may be inferred that these garnet portions were formed at several stages with different pressure conditions in the Wölz Complex. It must be noted, however, that reactions with a Ca-bearing accessory phase and/or pre-existing chemical heterogeneities may also influence the grossular content of the first garnet growth increments. In contrast, all garnet cores appear to have been formed at a single stage of their polymetamorphic evolution in the Rappold Complex.

Garnet from the Wölz Complex

The application of garnet isopleth thermobarometry to the central portions of all the first-generation garnet

studied (Fig. 15) testifies to garnet growth at relatively low pressures during the Permian metamorphic event with a geotherm of $\sim 40^\circ\text{C km}^{-1}$.

The Cretaceous second-generation garnet is considered problematic in the context of garnet isopleth thermobarometry because it forms overgrowths on pre-existing garnet, i.e. it grew in rocks, which already contained garnet that was formed during pre-Eo-Alpine stages. These rocks underwent substantial dehydration during pre-Eo-Alpine times and the extent of chemical equilibration, i.e. the size of equilibration domains that developed during the Eo-Alpine event is not known. However, the area of isopleth intersection obtained for the first-growth increments of the second-generation garnet considering garnet fractionation is small (Fig. 12). In addition, the calculated equilibrium-phase assemblage is observed as mineral inclusions in the second-generation garnet with the exception of chlorite and plagioclase, which might have been part of the matrix. Hence, the pronounced difference in the composition of the oldest growth increment of the Permian first-generation garnet and of the Eo-Alpine second-generation garnet is interpreted to reflect a pressure difference of ~ 2 kbar between the Permian and Eo-Alpine metamorphic events, at least during the stages of incipient garnet growth.

The most promising candidate for garnet isopleth thermobarometry on Eo-Alpine parageneses is garnet from the Wölz Complex with a single growth zone. As shown in Fig. 15, conditions of 6.5 ± 0.5 kbar and $540 \pm 10^\circ\text{C}$ are obtained for their incipient formation.

The similarities of the P - T conditions indicated for incipient growth of garnet with a single growth zone and those indicated for the earliest growth stages of the second-generation garnet confirm that both were formed during the same Eo-Alpine metamorphic event. During the incipient growth stages of Eo-Alpine garnet, the geothermal gradient was at $\sim 20^\circ\text{C km}^{-1}$. This is markedly lower than a thermally relaxed continental geotherm and indicates that Eo-Alpine garnet started to grow during a fast subduction process, where thermal relaxation could not keep up with rapid pressure increase.

Garnet from the Rappold Complex

Garnet isopleth thermobarometry applied to the oldest growth increments of first-generation garnet yields P - T conditions of 5.3 ± 0.3 kbar and $525 \pm 15^\circ\text{C}$ (Fig. 15). These temperatures are within uncertainties identical to those obtained by Faryad & Hoinkes (2003). The pressures, however, are lower by ~ 1.3 kbar. The fact, that this garnet constitutes a group, which is clearly separated in P - T space from the first-generation, low-pressure garnet from the Wölz Complex, suggests that they pertain to a different metamorphic event, possibly of Variscan age. Alternatively, the garnet cores of the Rappold Complex

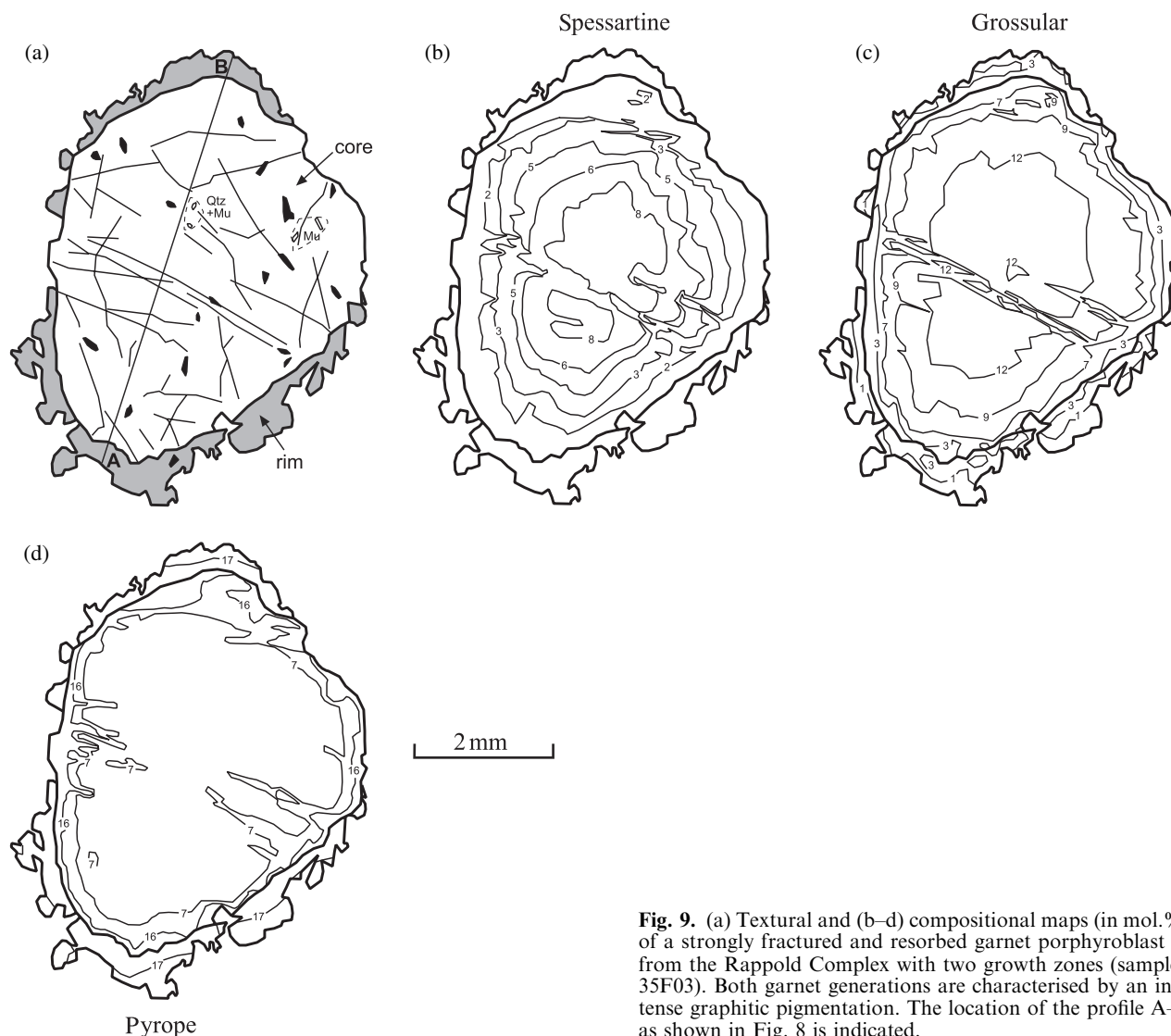


Fig. 9. (a) Textural and (b–d) compositional maps (in mol.%) of a strongly fractured and resorbed garnet porphyroblast from the Rappold Complex with two growth zones (sample 35F03). Both garnet generations are characterised by an intense graphitic pigmentation. The location of the profile A–B as shown in Fig. 8 is indicated.

may also have formed during the Permian but in a different crustal segment than the first-generation garnet of the Wölz Complex. According to our P – T estimates, the geothermal gradient was at ~ 30 °C km $^{-1}$ during this pre-Eo-Alpine event.

Chemical zoning of garnet and estimated P – T paths for progressive garnet growth

The general zoning patterns observed in garnet porphyroblasts from the Rappold and Wölz Complexes, in particular, the bell-shaped distribution of X_{sps} (Figs 4, 6 & 8) are typical for garnet growth under greenschist and amphibolite facies conditions during a prograde P – T path (e.g. Hollister, 1966; Tracy *et al.*, 1976; Spear, 1993). The successive outward decrease of X_{sps} reflects the progressive Mn depletion of the matrix caused by fractionation of Mn into garnet. Depending on the P – T path, certain components such as Mg or Fe

tend to be preferentially fractionated into garnet as well. By this mechanism, the thermodynamically relevant bulk composition can substantially change during garnet growth. As shown in Fig. 10, the compositions of the garnet cores from the Wölz and Rappold Complexes differ significantly from the average bulk-rock compositions. This implies that the composition of the equilibrium domain was progressively changed by chemical fractionation during garnet growth especially if the modal percentage of newly formed garnet was high.

To account for the effects of chemical fractionation during garnet growth, the fractionation model of Evans (2004) was employed to estimate the P – T conditions during garnet growth although the distribution coefficient of MnO between garnet and the rock matrix cannot be assumed constant as the temperature changes and the composition of the garnet-bearing phase assemblage is possibly modified during

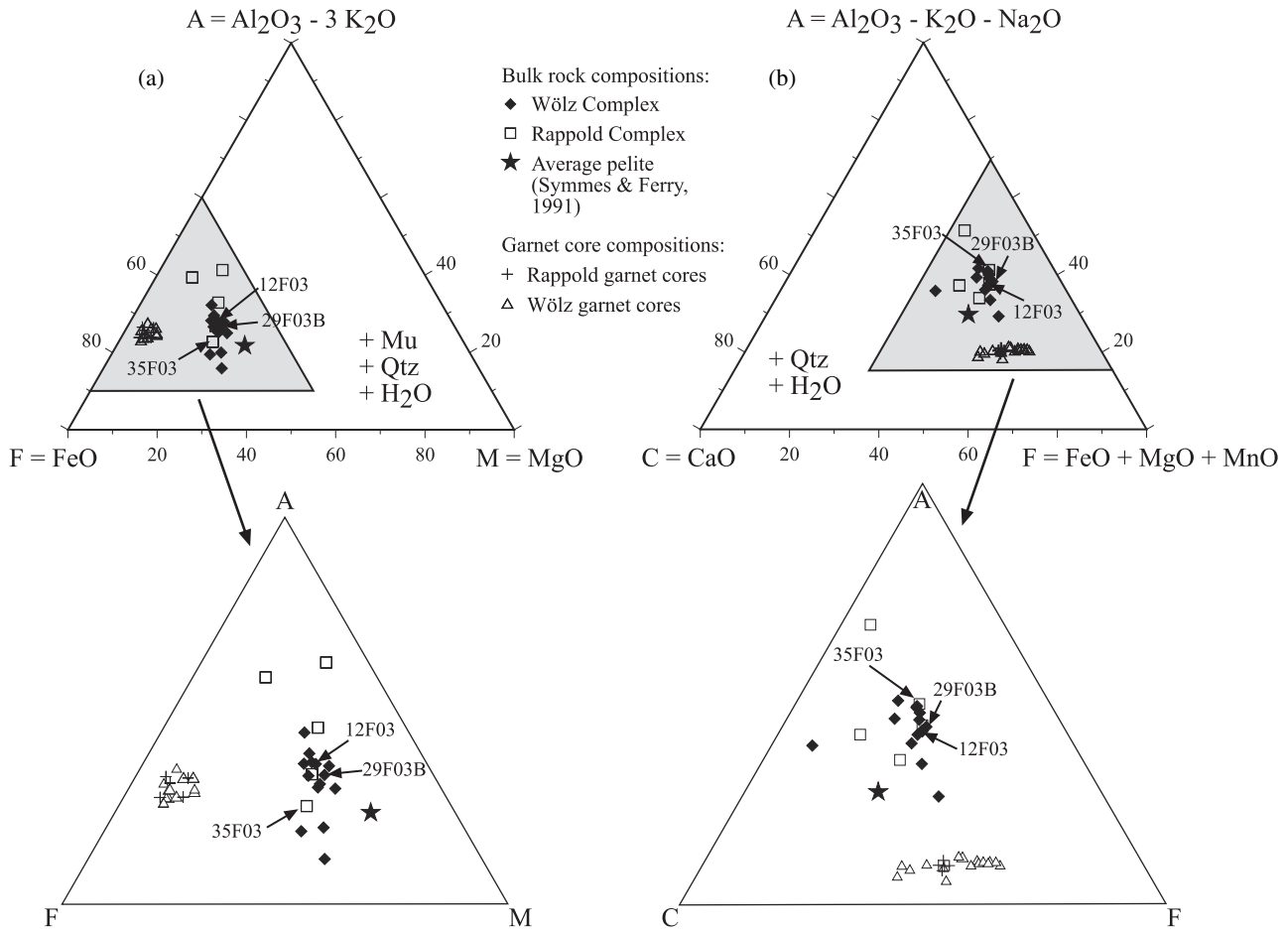


Fig. 10. Bulk-rock XRF geochemical data and garnet core compositions of all the samples used for garnet isopleth thermobarometry plotted in an (a) AFM projection from muscovite, quartz and H₂O (Thompson, 1957) and (b) ACF projection from quartz and H₂O. Total iron in all samples is assumed to be FeO.

garnet evolution. In spite of this insufficiency, the obtained areas of isopleth intersection are small (Figs 12d, 13d & 14d). This indicates that the fractionation model correctly describes the modification of the thermodynamically relevant bulk composition associated with garnet growth for the samples studied.

Two-phase garnet from the Wölz Complex

The almost euhedral growth zoning pattern of the Permian first-generation garnet documented by the spessartine isopleths (Fig. 5) indicates the preservation of the primary zoning pattern. Only the 0.08 X_{sps} isopleth shows a local irregularity, which is probably caused by a late-stage alteration along a crack. The smooth zoning of the major components (Fig. 4) reflects growth in the course of temporally continuous reactions, where the nutrients for garnet formation were continuously liberated by the breakdown of the precursor phases and transported to the sites of garnet formation.

The P – T path for the formation of the entire first-generation garnet obtained by garnet isopleth thermobarometry and the fractionation model of Evans (2004) is relatively flat [points (1) to (3) in Fig. 12d]. The areas of isopleth intersection are comparatively small and the predicted influence of garnet fractionation on garnet stability and composition is almost negligible even for the last growth stage of garnet growth. It is interesting to note that garnet growth along such a P – T path produces a successive decrease in X_{grs} despite growth during slightly increasing pressure.

The equilibrium phase assemblage predicted for the three garnet growth stages [points (1) to (3) in Fig. 12e] is not completely preserved as inclusions in the first-generation garnet. Only ilmenite, quartz, muscovite and tourmaline inclusions are observed. Chlorite, staurolite and albite-rich plagioclase are interpreted to have been part of the Permian matrix assemblage. The P – T estimates for incipient and progressive growth increments of the first-generation garnet support the hypothesis of a Permian extensional event for this part

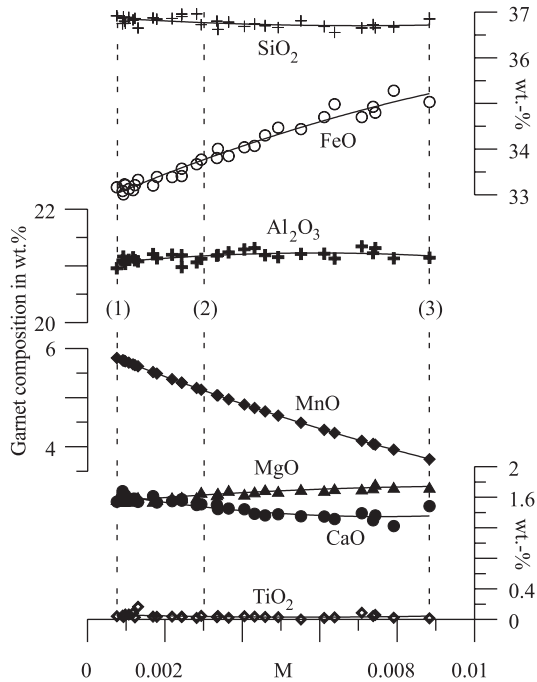


Fig. 11. Relationship between M (weight fraction of crystallized garnet) and the chemical composition of the successive growth increments of first-generation garnet from the Wölz Complex (sample 12F03). Points (1), (2) and (3) correspond to the garnet points in Fig. 4. For k_d (distribution coefficient of MnO) a value of 55 was used.

of the Austroalpine Basement (e.g. Miller & Thöni, 1995; Schuster & Thöni, 1996; Schuster *et al.*, 2001).

The innermost portions of the Cretaceous second-generation garnet are characterized by a continuous increase of $\text{Fe}/(\text{Fe} + \text{Mg})$ from 0.93 to 0.94 and simultaneous decrease of X_{alm} , X_{prp} , and X_{sps} and concomitant increase of X_{grs} (see right-hand side of the profile in Fig. 4). According to Spear *et al.* (1991), this may be interpreted as a result of garnet growth during increasing pressure and decreasing temperature conditions. Such a P - T trajectory would, however, imply a very special tectonic evolution, which is not known for the Eo-Alpine orogenic event in the Eastern Alps. Alternatively, the peculiar zoning pattern may be explained by modification through diffusional exchange across the interface between first and second growth stage of garnet porphyroblasts. The 'shoulder' in the X_{grs} trend (Fig. 4) defines a separate stage of second-generation garnet growth. This feature is observed in almost every second-generation garnet from polyphase garnet of the Wölz Complex. It reflects a period of enhanced availability of calcium, which may be due to the breakdown of a Ca-bearing phase such as epidote rather than large changes in P - T conditions. The decrease in X_{prp} and concomitant increase in $\text{Fe}/(\text{Fe} + \text{Mg})$, which is observed in the outermost portions of the second-generation garnet, is ascribed to diffusive Fe-Mg exchange between garnet and matrix

phases during retrogression. Hence, the compositions of the outermost garnet rims cannot be considered as equilibrium relations at peak metamorphic conditions. They reflect the element partitioning between garnet and matrix phases at some stage during cooling, which makes it difficult to apply conventional thermobarometry to these rocks.

Quantitative information about the P - T conditions during progressive growth of the Cretaceous second-generation garnet, which rims the Permian first-generation garnet, could not be obtained employing garnet isopleth thermobarometry and the fractionation model. The areas of isopleth intersection are large and the uncertainties in P - T estimates are accordingly large for the outermost portions of Eo-Alpine garnet. This is, at least in part, due to the fact that the X_{alm} -, X_{sps} - and X_{grs} -isopleths tend to become parallel to each other and become pressure-independent at pressures in excess of ~ 7 kbar (Fig. 12). In addition, as mentioned above, the size of equilibration domains may have been rather limited during the Eo-Alpine metamorphic overprint in the rocks, which already had experienced earlier medium-grade metamorphism. This is why bulk-rock compositions combined with a simple fractionation model are no longer an adequate description of the thermodynamically relevant bulk composition. Disequilibrium between the garnet rim and the matrix phases at later stages of garnet growth can also be invoked.

Nevertheless, qualitative information on the P - T conditions during the growth of the second-generation garnet can be deduced from the calculated phase relations in Fig. 12. The local maximum in X_{alm} in the outer part of the second-generation garnet (Fig. 4) indicates that the rocks followed a P - T path, which passes through the predicted maximum in X_{alm} (Fig. 12a). The existence of a local maximum in X_{alm} in P - T space is predicted for all bulk-rock compositions investigated in this study. It generally falls into the chlorite stability field and approximately coincides with the low-temperature stability limit of biotite (Figs 12, 13 & 14). A chemical zoning pattern similar to that of the second-generation garnet from the Wölz Complex (Fig. 4), in particular, a maximum in X_{alm} combined with a concomitant decrease of X_{grs} and $\text{Fe}/(\text{Fe} + \text{Mg})$ was obtained by Spear *et al.* (1991) from numerical simulations that implied increasing pressures and temperatures during garnet growth. Such zoning patterns have also been reported from several other prograde garnet growth stages by Vance & Holland (1993) and by Vance & Mahar (1998) and interpreted as a primary, reaction-controlled feature. From a simulation of garnet growth at the expense of chlorite, Inui & Toriumi (2004) suggest that the rapid rise of X_{Mg} and the concomitant decrease in X_{alm} is due to an increase in the relative amounts of clinocllore [$\text{Mg}_5\text{Al}_2\text{Si}_3\text{O}_{10}(\text{OH})_8$] and amesite [$\text{Mg}_4\text{Al}_4\text{Si}_2\text{O}_{10}(\text{OH})_8$] and a decrease of daphnite [$\text{Fe}_5\text{Al}_2\text{Si}_3\text{O}_{10}(\text{OH})_8$] in chlorite with increasing temperature.

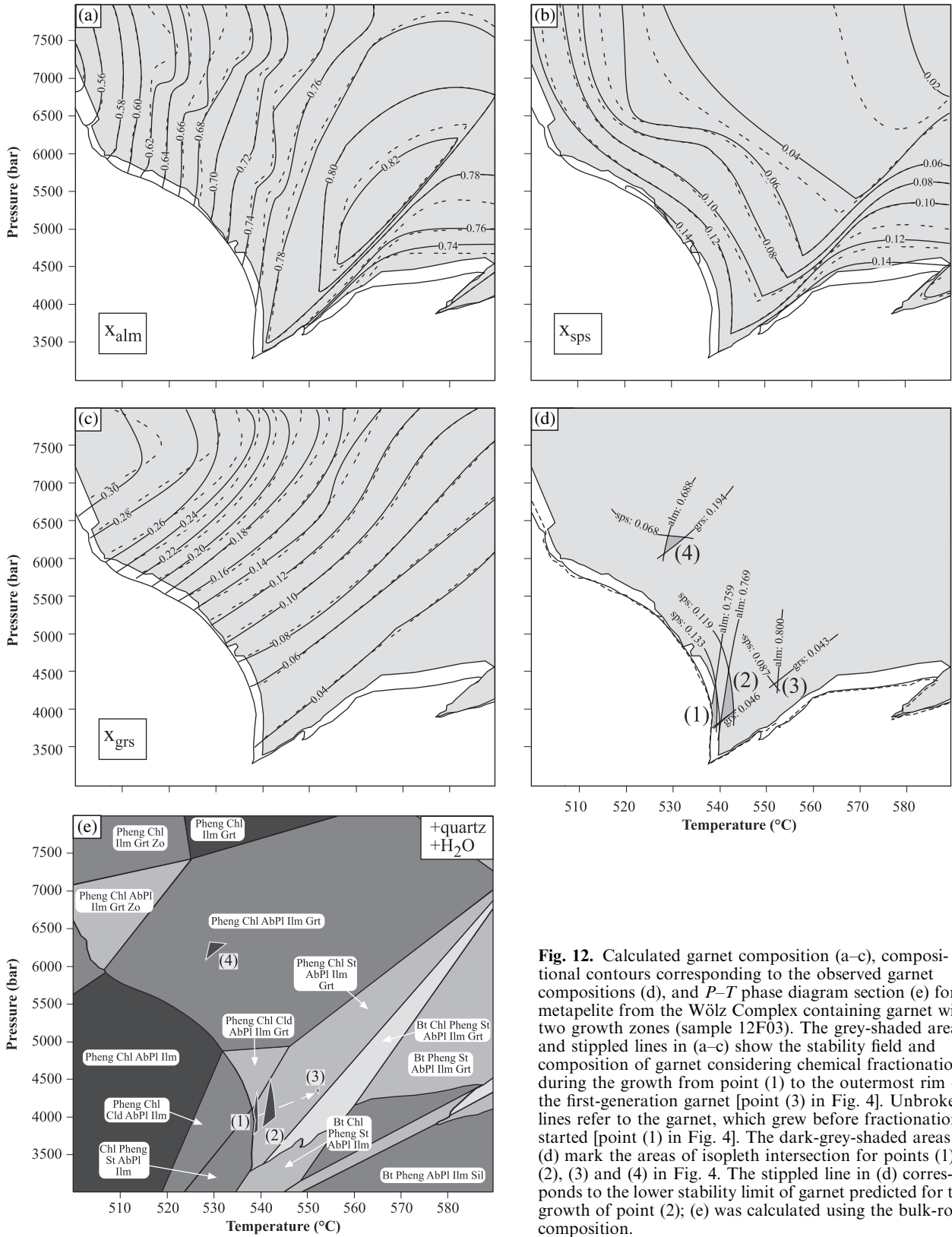


Fig. 12. Calculated garnet composition (a–c), compositional contours corresponding to the observed garnet compositions (d), and P – T phase diagram section (e) for a metapelite from the Wölz Complex containing garnet with two growth zones (sample 12F03). The grey-shaded area and stippled lines in (a–c) show the stability field and composition of garnet considering chemical fractionation during the growth from point (1) to the outermost rim of the first-generation garnet [point (3) in Fig. 4]. Unbroken lines refer to the garnet, which grew before fractionation started [point (1) in Fig. 4]. The dark-grey-shaded areas in (d) mark the areas of isopleth intersection for points (1), (2), (3) and (4) in Fig. 4. The stippled line in (d) corresponds to the lower stability limit of garnet predicted for the growth of point (2); (e) was calculated using the bulk-rock composition.

The position of the high-pressure limit of the X_{alm} -maximum is slightly shifted to higher pressures because of chemical fractionation associated with garnet growth (Figs 12a, 13a & 14a). In contrast, the position of the low-pressure limit is not affected. Garnet, which grew in a similar chemical system but at higher pressure than the second-generation garnet from the Wölz Complex may pass by the predicted maximum in X_{alm} and thus lack the local X_{alm} -maximum in their chemical zoning pattern.

One-phase garnet from the Wölz Complex

The X-ray maps of the Cretaceous one-phase garnet show the modifying influence of crack formation and mineral inclusions on the original garnet growth zoning (Fig. 7). The relatively high number of mineral inclusions compared with those in the Cretaceous second-generation garnet of the Wölz Complex and the fluctuations of X_{alm} and X_{grs} may be due to a slightly different mineralogical composition of the preexisting matrix at the site of garnet formation or to a higher rate of garnet growth. Assuming similar values of volume garnet growth, the extent of radial garnet growth strongly depends on the size of the grain, which is overgrown. Hence, the rate of radial garnet growth would be faster for the formation of the one-phase garnet than for the formation of the second-generation garnet of the polyphase garnet porphyroblasts, which forms rims around preexisting garnet grains.

Considering garnet fractionation (Evans, 2004), a P - T path for the core formation of the Cretaceous one-phase garnet [points (1) to (3) in Fig. 6] is obtained, which passes by the predicted maximum in X_{alm} (Fig. 14). Therefore, the garnet lacks a local maximum in X_{alm} in its zoning pattern. The P - T path is comparatively steep, which is in line with the hypothesis of garnet growth during an Eo-Alpine subduction process.

The modelled equilibrium-phase assemblage for the oldest garnet portion [point (1) in Figs 6 & 14e] agrees exactly with the paragenesis predicted for the formation of point (2) (Figs 6 & 14e), and the influence of garnet fractionation on garnet composition and stability during this garnet growth stage is insignificant. In contrast, fractionation throughout the last growth stage [point (2) to (3) in Figs 6 & 14f] results in a remarkable change of the phase diagram topology.

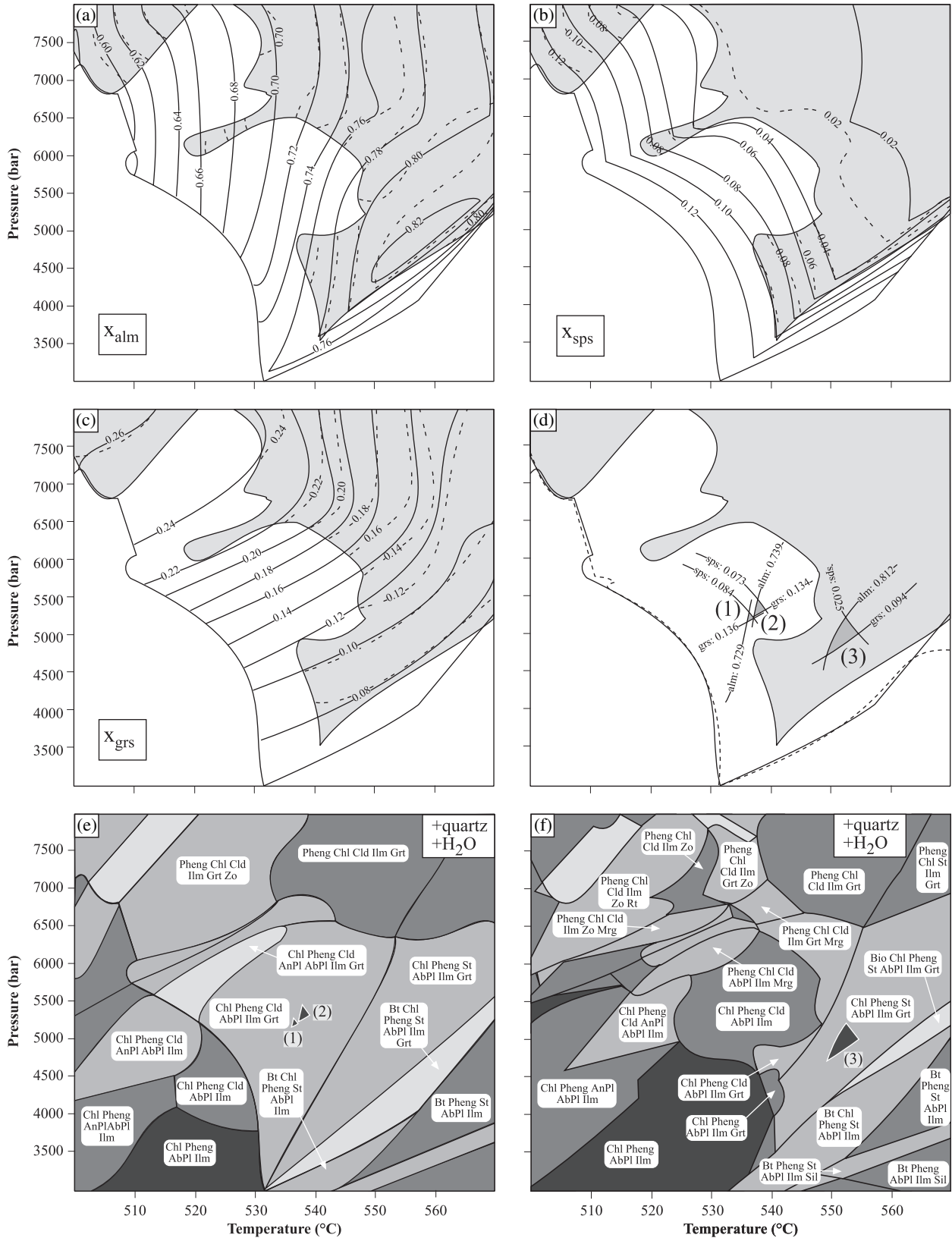
Allanite and clinozoisite inclusions are observed in central parts of garnet but are not predicted as stable phases employing garnet isopleth thermobarometry and garnet fractionation [points (1) to (3) in Fig. 14]. Both phases are members of the epidote group, which is approximated as zoisite in the calculations. The areas of isopleth intersection for points (1), (2) and (3) are positioned at somewhat lower pressures or slightly higher temperatures than the stability limit of zoisite-bearing assemblages (Fig. 14f). We attribute this discrepancy to reflect differences in the thermodynamic properties of clinozoisite and allanite compared with zoisite. Kyanite and rutile inclusions are noticed in the outermost garnet rim, which grew subsequently to the formation of the youngest garnet growth stage considered [point (3) in Figs 6 & 14e]. Therefore, we suggest the formation of rutile and kyanite as well as staurolite, which is commonly intergrown with kyanite in the matrix, during and following the latest periods of Cretaceous garnet growth accounting for their absence in the phase assemblages modelled.

The P - T conditions obtained for the growth of the second-generation garnet from the Wölz Complex represent parts of a Cretaceous prograde P - T path in the course of Eo-Alpine metamorphism. However, peak metamorphic conditions for the Eo-Alpine event could not be obtained. They are expected to exceed the maximum conditions achieved for the growth of the one-phase garnet from the Wölz Complex. In this respect, they would be in accordance with thermobarometrical estimates of ~ 10 – 11 kbar and 600 – 650 °C obtained for peak metamorphic conditions during Eo-Alpine metamorphism in the Wölz Complex by Faryad & Hoinkes (2003). Koroknai *et al.* (1999) obtained conditions of 10 kbar and 600 °C for metapelites from the southernmost section of the Wölz Complex (Radenthein Complex; Fig. 1). In contrast, peak metamorphic conditions for the central parts of the Wölz Complex (Ramingstein Window; Fig. 1) were estimated at ~ 7 kbar and 570 °C by Schuster & Frank (1999).

Polyphase garnet from the Rappold Complex

The compositional heterogeneity of the first-generation garnet (Fig. 8) may be due to the inheritance of preexisting chemical heterogeneities, or to late-stage diffusional modification of the chemical composition of garnet adjacent to cracks and mineral inclusions (Fig. 9). A condensation of the X_{sps} isopleths in the

Fig. 13. Calculated garnet composition (a–c), compositional contours corresponding to the observed garnet compositions (d), and P - T phase diagram sections (e–f) for a metapelite from the Rappold Complex containing garnet with two growth zones (sample 35F03). The grey-shaded area and stippled lines in (a–c) show the stability field and composition of garnet considering chemical fractionation during the growth from point (1) to point (3) in Fig. 8. Unbroken lines refer to the garnet, which grew before fractionation started [point (1) in Fig. 8]. The dark-grey-shaded areas in (d) mark the areas of isopleth intersection for points (1), (2) and (3) in Fig. 8. The stippled line in (d) corresponds to the lower stability limit of garnet predicted for the growth of point (2); (e) and (f) were calculated using the bulk-rock chemistry as the composition of the thermodynamic system at the initial stage of garnet growth and the calculated effective composition for garnet growth stage (3), respectively.



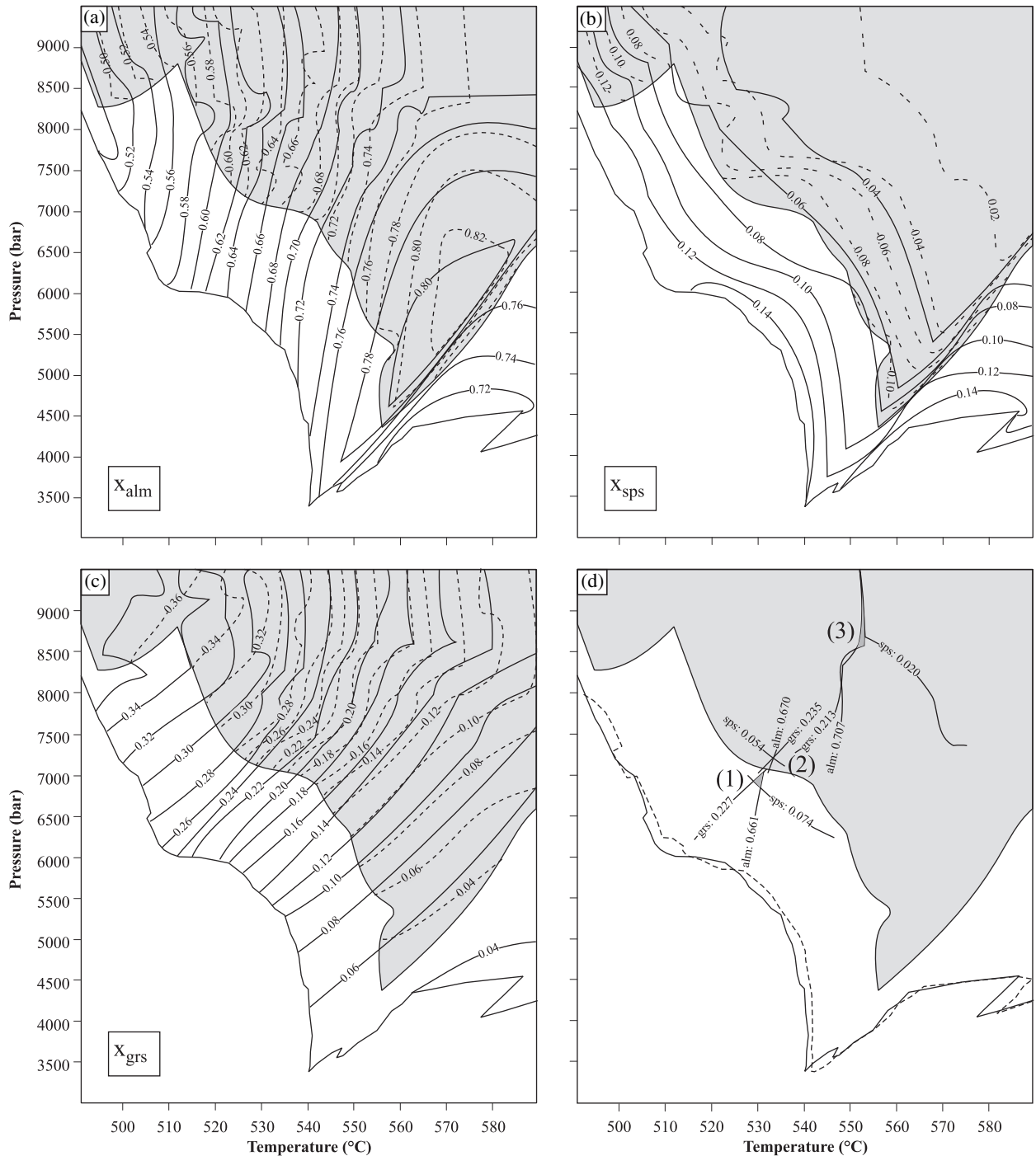


Fig. 14. Calculated garnet composition (a–c), compositional contours corresponding to the observed garnet compositions (d), and P – T phase diagram sections (e–f) for a metapelite from the Wölz Complex containing garnet with a single growth zone (sample 29F03B). The grey-shaded area and stippled lines in (a–c) show the stability field and composition of garnet considering chemical fractionation during the growth from point (1) to point (3) as shown in Fig. 6. Unbroken lines refer to the garnet which grew before fractionation started [point (1) in Fig. 6]. The dark-grey-shaded areas in (d) mark the areas of isopleth intersection for points (1), (2) and (3) in Fig. 6. The stippled line in (d) corresponds to the lower stability limit of garnet predicted for the growth of point (2); (e) and (f) were calculated using the bulk-rock chemistry as the composition of the thermodynamic system at the initial stage of garnet growth and the calculated effective chemical composition at garnet growth stage (3), respectively.

upper right portion of the garnet core is observed, which probably reflects a period of garnet resorption (Fig. 9). The sharp increase of $Fe/(Fe + Mg)$ and

concomitant decrease in X_{prp} in the outermost 10–20 μm is supposed to indicate retrograde diffusional exchange with matrix phases.

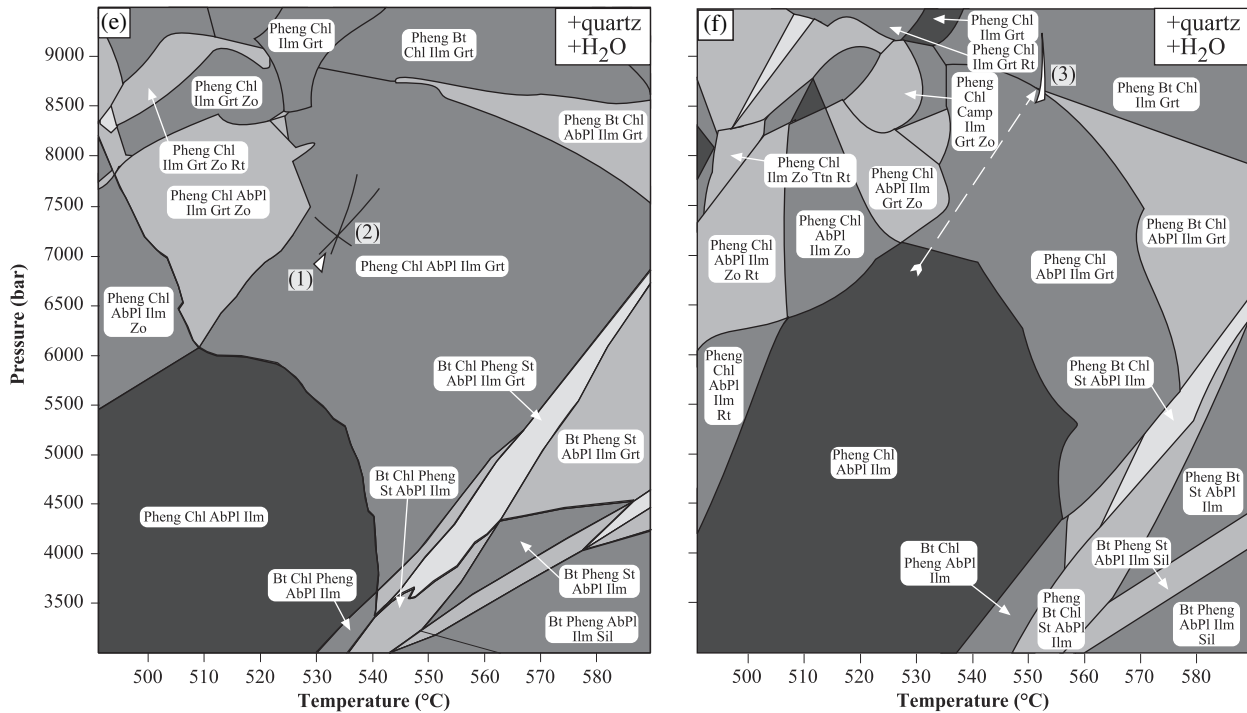


Fig. 14. *Cont'd.*

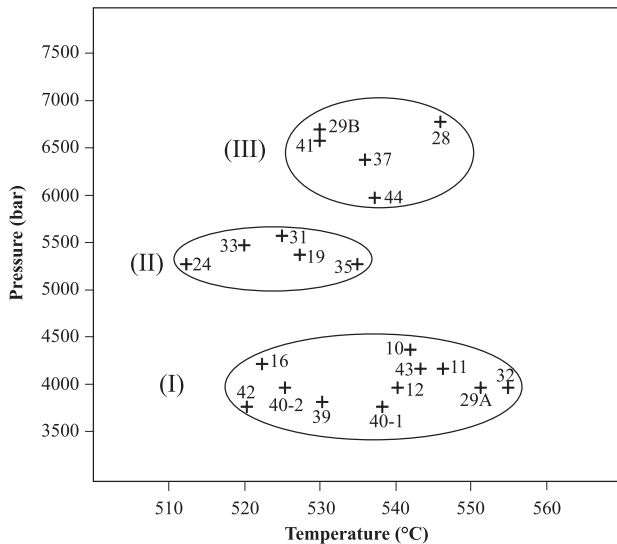


Fig. 15. Summary of the P - T estimates for the incipient stages of garnet growth in metapelites obtained from the Wölz and Rappold Complexes. (i) First-generation garnet of Permian age from the Wölz Complex; (ii) first-generation garnet of unknown age from the Rappold Complex; (iii) garnet with a single growth zone of Cretaceous age from the Wölz Complex. Geographical position of the samples is given in Table 1 and Fig. 2. The respective areas of isopleth intersection are provided in Appendix A3 for the entire set of samples.

It is interesting to note that Mn is not entirely depleted from the rock matrix even during the latest growth increments of the first-generation garnet

(Fig. 8). This points to the presence of an additional Mn-bearing phase, which acted as a source of Mn even after chlorite has been entirely consumed in the course of garnet growth.

The resulting P - T path for the growth of the central part of the first-generation garnet proposes garnet formation at increasing temperature and constant or even decreasing pressure (Fig. 13d). The estimated P - T path is aimed at the local maximum in X_{alm} that is predicted for the respective bulk-rock composition (see Fig. 13a). The reversal trend of X_{alm} in the compositional profile (Fig. 8) implies that this feature is passed through at later growth stages.

With the exception of chlorite and plagioclase, all the predicted minerals are perceived as inclusions in early portions of the first-generation garnet. Chemical fractionation in the course of garnet growth noticeably changes the topology of the predicted-phase assemblage relations (Fig. 13e,f). At point (3), staurolite is calculated to be stable (Fig. 13f) and probably corresponds to the strongly resorbed staurolite porphyroblasts noticed in thin sections, which enclose first-generation garnet and form equilibrium textures with them (Fig. 3c). Biotite, which is observed in the outermost portions of the first-generation garnet, was not predicted as part of the paragenesis at point (3). However, the position of the lower stability limit of biotite is located at slightly higher temperatures as calculated for the formation of point (3) (Fig. 13f). Hence, biotite might be part of an equilibrium assemblage at later stages of garnet

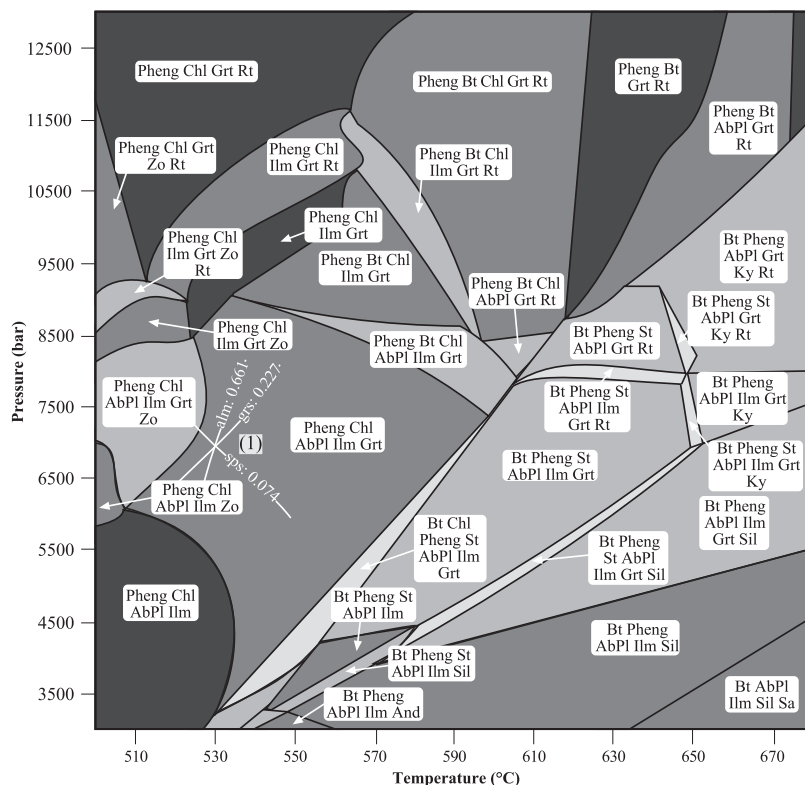


Fig. 16. P - T phase diagram section for incipient garnet growth in a metapelite from the Wölz Complex containing garnet porphyroblasts with a single growth zone (sample 29F03B) considering a GCOH-fluid (Connolly & Cesare, 1993) (for further explanation see text).

growth, which evolves, if the rock follows a P - T path proceeding through the maximum in X_{alm} .

The influence of Ti-biotite and the composition of the fluid

The comparison of P - T phase diagram sections obtained by the implementation of the Ti-free and Ti-bearing solution model of biotite (Powell & Holland, 1999) yields a slightly increased stability of garnet in equilibrium assemblages with Ti-biotite, e.g. consideration of Ti in biotite shifts the garnet-in curve to slightly lower pressures at temperatures exceeding the lower stability limit of biotite. However, the chemical composition of garnet is not affected. As incipient garnet growth is assumed to occur at the expense of chlorite, the influence of Ti-biotite on the stability of garnet can be ignored in this case.

To assess the influence of changing H_2O and CO_2 activities during garnet growth on garnet composition and phase diagram topology and to account for the remarkable amount of graphite observed in the garnet porphyroblasts studied, a P - T phase diagram section was calculated (Fig. 16) considering a graphite-buffered carbon-, oxygen- and hydrogen-bearing (GCOH-) fluid (Connolly & Cesare, 1993). At pressures of ~ 3.5 kbar, the lower stability limit of garnet is shifted to lower temperatures by ~ 10 °C compared with the respective equilibrium-phase assemblage diagram calculated with pure H_2O (Fig. 14e) whereas the composition of garnet was not changed. However, the

influence of fluid composition on garnet stability decreases as the pressure increases. At pressures exceeding 6 kbar, the phase diagram topologies illustrated in Figs 14e & 16 match exactly. Figure 16 also shows the area of isopleth intersection for incipient garnet growth in sample 29F03B. The P - T conditions obtained correspond to the P - T estimates acquired using pure H_2O .

Limitations of garnet isopleth thermobarometry

The P - T conditions predicted for the growth of the most primitive garnet in samples 35F03 and 29F03B are not exactly located at the low-temperature, low-pressure stability limit of the garnet stability field (Figs 13f & 14f). Several possible mechanisms may be invoked to explain this apparent discrepancy: the position of the lower limit of the stability field of garnet strongly depends on the amount of Mn available for garnet growth. Thus, Mn-bearing phases that may coexist with garnet must be taken into account during thermodynamic modelling. If such phases are ignored or inadequately described thermodynamically, this may have a strong influence on the stability field of garnet. The application of different solution models for solid solution in feldspar (Newton *et al.*, 1980; Baldwin *et al.*, 2005) clearly reflects that the quantity of Ca available for garnet growth strongly influences the position of the garnet-in curve. However, the choice of the feldspar model does not significantly alter the

position and shape of the garnet isopleths, e.g. the predicted composition of garnet is only slightly affected by the thermodynamic properties of feldspar solid solution. Furthermore, errors in experimentally obtained thermodynamic properties of minerals, which are introduced via the thermodynamic database used, have to be taken into account. Alternatively, reaction overstepping due to kinetically impeded nucleation and/or volume diffusion of Mn may be invoked. At the stage of incipient growth, the garnet individuals were supposedly very small, and the modal proportion of garnet in the rock can be neglected (Tables 5 & 6). It may be hypothesized that, despite the low temperatures, volume diffusion of Mn was fast enough to homogenize any growth zoning in garnet effectively, so that the entire grains could maintain an equilibrium distribution with the rock matrix in terms of their Mn concentrations. In this case, garnet isopleth thermobarometry yields valid P - T estimates for an early growth stage.

Of more than 40 samples investigated from both lithostratigraphic units, about 20 have not been deemed successful. In these cases, the areas of isopleth intersection cover more than ~ 1.5 kbar and ~ 20 °C, and are too large to obtain well-founded P - T estimates. The failure of garnet isopleth thermobarometry may be due to several reasons.

If the method is applied to late increments of garnet growth without consideration of the effect of chemical fractionation produced during preceding garnet growth, i.e. if bulk-rock chemistries are used for phase equilibrium calculations, this may result in enlarged areas of isopleth intersection and unsatisfactory precision of the method. In the case of garnet that grew under greenschist to amphibolite facies conditions, this may even lead to systematic underestimation of pressure and to overestimation of temperature, because of the characteristic growth zoning of such garnet.

Furthermore, the positions of the isopleths may tend to become parallel at high pressures as shown for the Cretaceous second-generation garnet of sample 12F03. This results in strongly extended areas of isopleth intersection and unsatisfactorily large P - T uncertainties for garnet grown at relatively high pressures.

In garnet isopleth thermobarometry, the bulk-rock composition or the effective bulk-rock composition is usually employed as the thermodynamically relevant system composition. This is valid as long as thermodynamic equilibrium is maintained over the entire rock volume considered at any time of garnet growth. In general, equilibration volumes will be of finite size, depending on the efficiency of mass transport in the rock matrix. Mass transfer in rocks may be slow so that a single rock specimen may contain several equilibration domains. Garnet cores in a rock sample which grew at the same metamorphic event and nucleate at similar times but differ strongly with respect to their chemical composition may be considered indicators for the juxtaposition of different equilibration

domains. In this case, the chemical composition of the rock sample averages out over the neighbouring equilibration domains and differs from the composition that is thermodynamically relevant for the growth of garnet within an individual equilibration domain.

The large number of fractures and mineral inclusions especially in garnet from the Rappold Complex are assumed to be responsible for secondary diffusional relaxation and modification of the original garnet composition. Moreover, garnet isopleth thermobarometry could not be applied to samples containing significant quantities of Fe^{3+} -bearing phases such as epidote or the garnet endmember andradite. An estimation of the original amounts of Fe_2O_3 at the time of incipient garnet growth could lead to more realistic models of rock-specific equilibrium-phase relations.

CONCLUSIONS

Estimates for the P - T conditions during incipient garnet growth and P - T trajectories representative for garnet growth in the course of pre-Eo-Alpine and Eo-Alpine metamorphic events in the Austroalpine basement are deduced from the investigation of bulk-rock chemistries and compositions of zoned metamorphic garnet porphyroblasts. The comparison of calculated garnet chemistries obtained from P - T phase diagram sections and garnet fractionation modelling with observed garnet compositions suggests different pre-Eo-Alpine metamorphic histories in the Wölz and Rappold Complexes. Whereas the Permian garnet from the Wölz Complex started to grow at $\sim 4 \pm 0.5$ kbar and 535 ± 20 °C incipient garnet growth of garnet from the Rappold Complex occurred at 5.3 ± 0.3 kbar and 525 ± 15 °C. The P - T estimates for the earliest growth zones of garnet from the Wölz Complex are in line with the presumed high temperature/low pressure conditions of the Permian metamorphic event. The P - T estimates for garnet from the Rappold Complex reflect a Barrow-type P - T path typical of Variscan metamorphism in the Eastern Alps. Investigations of Eo-Alpine garnet from the Wölz Complex yielded P - T conditions of 6.5 ± 0.5 kbar at 540 ± 10 °C during incipient garnet growth.

The typical growth zoning patterns observed in garnet of the Wölz and Rappold Complexes reflect changing component availabilities at the time of garnet growth. Besides garnet fractionation, component availability is controlled by several poorly constrained factors such as transport pathways and rates, the kinetics of decomposition reactions of precursor phases and garnet nucleation and growth, as well as diffusional relaxation. Therefore, the potential of garnet isopleth thermobarometry to derive P - T paths from zoning patterns is limited. In contrast, application of this technique to the first increments of garnet growth is reliable (e.g. Vance & Mahar, 1998; Stowell *et al.*, 2001; Zeh, 2001; Zeh & Holness, 2003; Evans, 2004).

The application of garnet isopleth thermobarometry together with garnet age determinations is suggested to be an efficient approach to obtain P - T - t information for the first metamorphic event of rocks that underwent a polymetamorphic evolution. In particular, it sheds light on pre-Eo-Alpine metamorphic events in the Austroalpine realm.

ACKNOWLEDGEMENTS

The authors thank W. Tschudin for the sample preparation, appreciate the editorial handling by M. Brown and D. Robinson and are grateful to D. K. Tinkham and A. Zeh for their thorough reviews. J. MacKenzie is thanked for language improvements.

REFERENCES

- Abart, R. & Martinelli, W., 1991. Variszische und alpidische Entwicklungsgeschichte des Wölzer Kristallins (Steiermark, Osterreich). *Mitteilungen der Gesellschaft der Geologie- und Bergbaustudenten in Osterreich*, **37**, 1–14.
- Atherton, M. P., 1968. The variation in garnet, biotite, and chlorite composition in medium grade pelitic rocks from the Dalradian, Scotland, with particular reference to the zonation in garnet. *Contributions to Mineralogy and Petrology*, **18**, 347–361.
- Ayres, M. & Vance, D., 1997. A comparative study of diffusion profiles in Himalayan and Dalradian garnets: constraints on diffusion data and the relative duration of the metamorphic events. *Contributions to Mineralogy and Petrology*, **128**, 66–80.
- Baldwin, J. A., Powell, R., Brown, M., Moraes, R. & Fuck, R. A., 2005. Modelling of mineral equilibria in ultrahigh-temperature metamorphic rocks from the Anápolis-Itaçu Complex, central Brazil. *Journal of Metamorphic Geology*, **23**, 511–531.
- Berman, R. G., 1988. Internally-consistent thermodynamic data for minerals in the system Na_2O - K_2O - CaO - FeO - Fe_2O_3 - Al_2O_3 - SiO_2 - TiO_2 - H_2O - CO_2 . *Journal of Petrology*, **29**, 445–552.
- Bernhard, F. & Hoinkes, G., 1999. Polyphase micaschists of the central Wölzer Tauern, Styria, Austria. 77 DMG conference MinWin 1999, Vienna. *Beihft European Journal of Mineralogy*, **11**, 22.
- de Capitani, C. & Brown, T. H., 1987. The computation of chemical equilibrium in complex systems containing non-ideal solutions. *Geochimica et Cosmochimica Acta*, **51**, 2639–2652.
- Carlson, W. D., 1989. The significance of intergranular diffusion to the mechanism and kinetics of porphyroblast crystallization. *Contributions to Mineralogy and Petrology*, **103**, 1–24.
- Carlson, W. D., 2001. Scales of disequilibrium and rates of equilibrium during metamorphism. *American Mineralogist*, **87**, 185–200.
- Chakraborty, S. & Ganguly, J., 1992. Cation diffusion in aluminosilicate garnets: experimental determination in spessartine-almandine diffusion couples, evaluation of effective binary, diffusion coefficients, and applications. *Contributions to Mineralogy and Petrology*, **111**, 74–86.
- Connolly, J. A. D., 1990. Multivariable phase diagrams: an algorithm based on generalized thermodynamics. *American Journal of Science*, **290**, 666–718.
- Connolly, J. A. D., 2005. Computation of phase equilibria by linear programming: a tool for geodynamic modeling and its application to subduction zone decarbonation. *Earth and Planetary Science Letters*, **236**, 524–541.
- Connolly, J. A. D. & Cesare, B., 1993. C-O-H-S fluid composition and oxygen fugacity in graphitic metapelites. *Journal of Metamorphic Geology*, **11**, 368–378.
- Connolly, J. A. D. & Petrini, K., 2002. An automated strategy for calculation of phase diagram sections and retrieval of rock properties as a function of physical conditions. *Journal of Metamorphic Geology*, **20**, 697–708.
- Dohmen, R. & Chakraborty, S., 2003. Mechanism and kinetics of element and isotopic exchange mediated by a fluid phase. *American Mineralogist*, **88**, 1251–1270.
- Evans, T. P., 2004. A method for calculating effective bulk composition modification due to crystal fractionation in garnet-bearing schist: implications for isopleth thermobarometry. *Journal of Metamorphic Geology*, **22**, 547–557.
- Faryad, S. W. & Hoinkes, G., 2003. P-T gradient of Eo-Alpine metamorphism within the Austroalpine basement units east of the Tauern Window (Austria). *Mineralogy and Petrology*, **77**, 129–159.
- Froitzheim, N., Schmid, S. M. & Frey, M., 1996. Mesozoic paleogeography and the timing of eclogite-facies metamorphism in the Alps: a working hypothesis. *Eclogae Geologicae Helvetiae*, **89**, 81–110.
- Gottschalk, M., 1997. Internally consistent thermodynamic data for rock-forming minerals in the system SiO_2 - TiO_2 - Al_2O_3 - CaO - MgO - FeO - K_2O - Na_2O - H_2O - CO_2 . *European Journal of Mineralogy*, **9**, 175–223.
- Griffen, D. T., 1981. Synthetic Fe/Zn staurolites and the ionic radius of IV Zn^{2+} . *American Mineralogist*, **66**, 932–937.
- Habler, G. & Thöni, M., 2001. Preservation of Permo-Triassic low-pressure assemblages in the Cretaceous high-pressure metamorphic Saualpe crystalline basement (Eastern Alps, Austria). *Journal of Metamorphic Geology*, **19**, 679–697.
- Hoinkes, G., Koller, F., Rantsch, G. et al., 1999. Alpine metamorphism of the Eastern Alps. *Schweizerische Mineralogische und Petrographische Mitteilungen*, **79**, 155–181.
- Holland, T. J. B. & Powell, R., 1998. An internally consistent thermodynamic data set for phases of petrological interest. *Journal of Metamorphic Geology*, **16**, 309–343.
- Holland, T. J. B., Baker, J. M. & Powell, R., 1998. Mixing properties and activity-composition relationships of chlorites in the system MgO - FeO - Al_2O_3 - SiO_2 - H_2O . *European Journal of Mineralogy*, **10**, 395–406.
- Hollister, L. S., 1966. Garnet zoning: an interpretation based on the Rayleigh fractionation model. *Science*, **154**, 1647–1651.
- Inui, M. & Toriumi, M., 2004. A theoretical study on the formation of growth zoning in garnet consuming chlorite. *Journal of Petrology*, **45**, 1369–1392.
- Kim, H. S. & Bell, T. H., 2005. Combining compositional zoning and foliation intersection axes (FIAs) in garnet to quantitatively determine early P-T-t paths in multiply deformed and metamorphosed schists: north central Massachusetts, USA. *Contributions to Mineralogy and Petrology*, **149**, 141–163.
- Kleemann, U. & Reinhardt, J., 1994. Garnet-biotite thermometry revisited: the effect of Al^{VI} and Ti in biotite. *European Journal of Mineralogy*, **6**, 925–941.
- Koroknai, B., Neubauer, F., Genser, J. & Topa, D., 1999. Metamorphic and tectonic evolution of Austroalpine units at the western margin of the Gurktal nappe complex, Eastern Alps. *Schweizerische Mineralogische und Petrographische Mitteilungen*, **79**, 277–295.
- Koziol, A. M. & Newton, R. C., 1988. Redetermination of the anorthite breakdown reaction and improvement of the plagioclase-garnet- Al_2SiO_5 -quartz geobarometer. *American Mineralogist*, **73**, 216–223.
- Koziol, A. M. & Newton, R. C., 1989. Grossular activity-composition relationships in ternary garnets determined by reversed displaced-equilibrium experiments. *Contributions to Mineralogy and Petrology*, **103**, 423–433.
- Kretz, R., 1964. Analysis of equilibrium in garnet-biotite-sillimanite gneisses from Quebec. *Journal of Petrology*, **5**, 1–20.
- Mahar, E. M., Baker, J. M., Powell, R., Holland, T. J. B. & Howell, N., 1997. The effect of Mn on mineral stability in metapelites. *Journal of Metamorphic Geology*, **15**, 223–238.

- Menard, T. & Spear, F. S., 1993. Metamorphism of calcic pelitic schists, Strafford Dome, Vermont: compositional zoning and reaction history. *Journal of Petrology*, **34**, 977–1005.
- Miller, C. & Thöni, M., 1995. Origin of eclogites from the Austroalpine Ötztal basement (Tirol, Austria): geochemistry and Sm-Nd vs. Rb-Sr isotope systematics. *Chemical Geology*, **122**, 199–225.
- Newton, R. C., Charlu, T. V. & Kleppa, O. J., 1980. Thermochemistry of the high structural state plagioclases. *Geochimica et Cosmochimica Acta*, **44**, 933–941.
- Powell, R. & Holland, T. J. B., 1993. An internally consistent dataset with uncertainties and correlations: 3. Applications to geobarometry, worked examples and a computer program. *Journal of Metamorphic Geology*, **6**, 173–204.
- Powell, R. & Holland, T. J. B., 1999. Relating formulations of the thermodynamics of mineral solid solutions: activity modeling of pyroxenes, amphiboles, and micas. *American Mineralogist*, **84**, 1–14.
- Proyer, A. & Dachs, E., 2000. Contrasting parageneses in mica schists of the Hohe Tauern, caused by manganese and zinc. *Mineralogy and Petrology*, **69**, 197–212.
- Schmid, S. M., Fügenschuh, B., Kissling, E. & Schuster, R., 2004. Tectonic map and overall architecture of the Alpine orogen. *Eclogae Geologicae Helveticae*, **97**, 93–117.
- Schuster, R. & Frank, W., 1999. Metamorphic evolution of the Austroalpine units east of the Tauern Window: indications for Jurassic strike slip tectonics. *Mitteilungen der Geologie- und Bergbaustudenten in Oesterreich*, **42**, 37–58.
- Schuster, R. & Thöni, M., 1996. Permian garnets: indication for a regional Permian metamorphism in the southern part of the Austroalpine basement units. *Mitteilungen der Österreichischen Mineralogischen Gesellschaft*, **141**, 219–221.
- Schuster, R., Scharbert, S., Abart, R. & Frank, W., 2001. Permo-Triassic extension and related HT/LP metamorphism in the Austroalpine-Southalpine realm. *Mitteilungen der Geologie- und Bergbaustudenten in Oesterreich*, **45**, 111–141.
- Schuster, R., Koller, F., Hoeck, V., Hoinkes, G. & Bousquet, R., 2004. Explanatory notes to the map: Metamorphic structure of the Alps - Metamorphic evolution of the Eastern Alps. *Mitteilungen der Österreichischen Mineralogischen Gesellschaft*, **149**, 175–199.
- Shaw, D. M., 1956. Geochemistry of pelitic rocks. Part III: Major elements and general geochemistry. *Geological Society of America Bulletin*, **67**, 919–934.
- Spear, F. S., 1993. *Metamorphic Phase Equilibria and Pressure-Temperature-Time Paths*. Mineralogical Society of America, Washington, D.C.
- Spear, F. S., Kohn, M. J., Florence, F. P. & Menard, T., 1991. A model for garnet and plagioclase growth in pelitic schists: implications for thermobarometry and P-T path determinations. *Journal of Metamorphic Geology*, **8**, 683–696.
- Stowell, H. H., Menard, T. & Ridgway, C. K., 1996. Ca-metasomatism and chemical zonation of garnet in contact-metamorphic aureoles, Juneau Gold Belt, southeastern Alaska. *Canadian Mineralogist*, **34**, 1195–1209.
- Stowell, H. H., Taylor, D. L., Tinkham, D. L., Goldberg, S. A. & Ouderkerk, K. A., 2001. Contact metamorphic P-T-t paths from Sm-Nd garnet ages, phase equilibria modelling and thermobarometry: garnet ledge, south-eastern Alaska, USA. *Journal of Metamorphic Geology*, **19**, 645–660.
- Symmes, G. H. & Ferry, J. M., 1991. Evidence from mineral assemblages for infiltration of pelitic schists by aqueous fluids during metamorphism. *Contributions to Mineralogy and Petrology*, **108**, 419–438.
- Symmes, G. H. & Ferry, J. M., 1992. The effect of whole-rock MnO content on the stability of garnet in pelitic schists during metamorphism. *Journal of Metamorphic Geology*, **10**, 221–237.
- Thompson, J. B., 1957. The graphical analysis of mineral assemblages in pelitic schists. *American Mineralogist*, **42**, 842–858.
- Thöni, M., 2002. Sm-Nd isotope systematics in garnet from different lithologies (Eastern Alps): age results, and an evaluation of potential problems for garnet Sm-Nd chronometry. *Chemical Geology*, **185**, 255–281.
- Tracy, R. J., Robinson, P. & Thompson, A. B., 1976. Garnet composition and zoning in the determination of temperature and pressure of metamorphism, central Massachusetts. *American Mineralogist*, **61**, 762–775.
- Vance, D. & Holland, T., 1993. A detailed isotopic and petrological study of a single garnet from the Gassetts Schist, Vermont. *Contributions to Mineralogy and Petrology*, **114**, 101–118.
- Vance, D. & Mahar, E., 1998. Pressure-temperature paths from P-T pseudosections and zoned garnets: potential, limitations and examples from the Zaskar Himalaya, NW India. *Contributions to Mineralogy and Petrology*, **132**, 225–245.
- Wei, C. J. & Powell, R., 2003. Phase relations in high-pressure metapelites in the system KFMASH (K₂O-FeO-MgO-Al₂O₃-SiO₂-H₂O) with application to natural rocks. *Contributions to Mineralogy and Petrology*, **145**, 301–315.
- White, R. W., Powell, R., Holland, T. J. B. & Worley, B. A., 2000. The effect of TiO₂ and Fe₂O₃ on metapelitic assemblages at greenschist and amphibolite facies conditions: mineral equilibria calculations in the system K₂O-FeO-MgO-Al₂O₃-SiO₂-H₂O-TiO₂-Fe₂O₃. *Journal of Metamorphic Geology*, **18**, 497–511.
- White, R. W., Powell, R. & Phillips, G. N., 2003. A mineral equilibria study of the hydrothermal alteration in mafic greenschist facies rocks at Kalgoorlie, Western Australia. *Journal of Metamorphic Geology*, **21**, 455–468.
- Zeh, A., 2001. Inference of a detailed P-T path from P-T pseudosections using metapelitic rocks of variable composition from a single outcrop, Shackleton Rang, Antarctica. *Journal of Metamorphic Geology*, **19**, 329–350.
- Zeh, A. & Holness, M. B., 2003. The effect of reaction overstep on garnet microtextures in metapelitic rocks on the Ilesha Schist Belt, SW Nigeria. *Journal of Petrology*, **44**, 967–994.
- Zeh, A., Millar, I. L. & Horstwood, M. S. A., 2004. Polymetamorphism in the NE Shackleton Range, Antarctica: constraints from petrology and U-Pb, Sm-Nd, Rb-Sr TIMS and in-situ U-Pb LA-PIMMS dating. *Journal of Petrology*, **45**, 949–973.

Received 27 October 2005; revision accepted 11 May 2006.

SUPPLEMENTARY MATERIAL

The following material is available online alongside the article at: <http://www.blackwell-synergy.com>:

Appendix A1. EPMA dataset.

Appendix A2. Bulk-rock compositions.

Appendix A3. P-T phase diagram sections with areas of isopleth intersection.

Appendix A4. The database file, one solution-model file, and one input-file used with PERPLEX.